APPENDIX B

PIPE-SYSTEM EXPERIMENT WITH AN ALTERNATIVE SIMULATED SEISMIC LOAD HISTORY

In the IPIRG-2 program two surface-cracked pipe-system experiments were conducted using a simulated seismic load history for the forcing function. For both experiments the test specimens contained internal circumferential surface cracks located at the same location as the cracks for the previously conducted IPIRG-1 pipe-system experiments. The cracked test specimens for these two IPIRG-2 pipe-system experiments were sections of A106 Grade B carbon steel and Type 304 stainless steel.

Of note from the analysis of these experiments was the fact that the load-carrying capacities of the simulated seismic experiments were higher than anticipated. There did not seem to be much of an effect of the cyclic history on the load-carrying capacity of the cracked section. One possible explanation for this observation was that the seismic history applied had a large cycle earlier in the time history, see Figure B.1, which resulted in a large moment cycle to occur at the crack section early in the experiment. It was during this large moment cycle that the crack initiated and began to grow. Consequently, the resultant moment-time history for the crack section looked very much like a dynamic-monotonic load history, see Figure B.2. As can be seen in this figure there were a number of small elastic cycles, very early in the time history, then the one large plastic cycle, during which the crack initiated, followed by another series of elastic cycles.

As a result, it was thought that the effects of cyclic loading due to a seismic loading event may not have been properly evaluated in these experiments. As such, it was decided to conduct a third surface-cracked simulated seismic pipe-system experiment as part of the BINP program with an alternative simulated seismic forcing function. The alternative seismic history would be designed such that there were more plastic cycles prior to crack initiation. This appendix describes the design of this alternative seismic history as well as presents the results and the analysis of this experiment.

B.1 DESIGN OF ALTERNATIVE SIMULATED SEISMIC FORCING FUNCTION

B.1.1 Background

Design of the forcing function used in the IPIRG-2 experiments was a well-considered process (Ref. B.1) using the following design criteria:

- Used accepted nuclear plant seismic design procedures
- Met various seismic regulatory guideline performance criteria
- Met TAG desires for percentage of inertial loading and stress ratio
- Seemed rational when compared with other seismic "floor" excitations
- Fit within the loading capabilities of the IPIRG pipe loop test system
- Was suitable for all of the IPIRG-2 simulated seismic experiments.

Although the IPIRG-2 forcing function met all of the design criteria, it did have the one previously mentioned deficiency that was not recognized until after all the experiments had been completed: the forcing function was not very challenging in terms of cyclic damage effects.

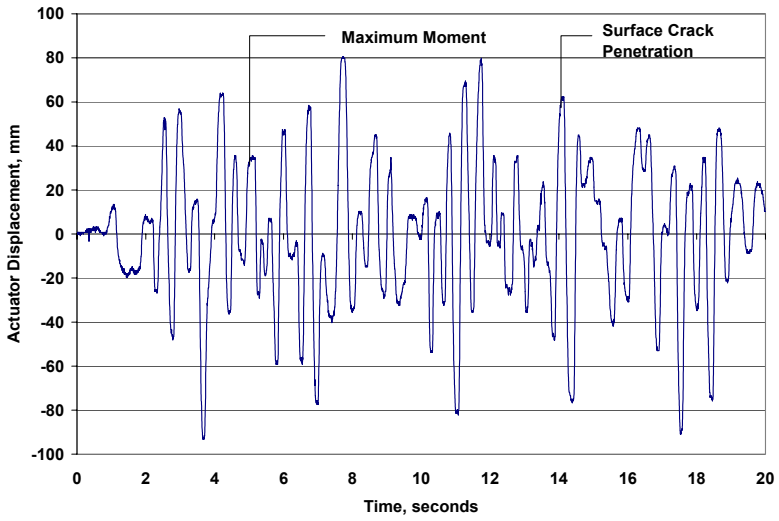

Figure B.1 Actuator displacement-time history for IPIRG-2 simulated seismic forcing function for stainless steel base metal experiment (Experiment 1-1)

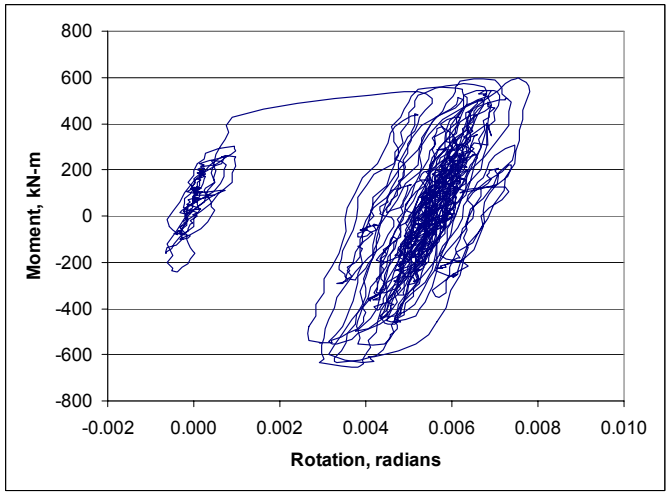

Figure B.2 Moment-rotation response for IPIRG-2 simulated seismic forcing function for stainless steel base metal experiment (Experiment 1-1)

Task 2 of the Battelle Integrity of Nuclear Piping (BINP) Program provided an opportunity to revisit the issue of the effects of cyclic, variable-amplitude, multi-frequency loading on the behavior of cracked pipe. Thus, in light of the understanding of cyclic and dynamic damage mechanisms that eventually existed at the end of the IPIRG-2 program, the BINP TAG members decided to conduct another simulated-seismic loading test in the IPIRG pipe-loop facility with a seismic forcing function that would be more challenging to the crack.

B.1.2 Design Issues for the BINP Seismic Forcing Function

The design of a seismic forcing function involves two distinct elements: 1) the selection of the loading and, 2) the analysis of the effect of the seismic loading on the cracked pipe. Because cracked pipe behavior is nonlinear, the

analysis must be done in the time domain to capture all of the load history effects and this, in turn, requires that the loading be defined in terms of a time history. Thus, the objective for the design of the BINP simulated-seismic forcing function was to find a "seismically inspired" time history of the pipe-loop system actuator motion that was potentially more damaging to a cracked pipe than the IPIRG-2 seismic time history.

Within this rather broad prescription for the design process, there are three basic issues that need to be considered:

1. The approach used to design the loading,
2. Material response issues, and
3. The implementation of the material response in the nonlinear analysis.

Each of these issues played a significant role in coming up with the final design for the BINP seismic forcing function and thus, deserves to be documented.

B.1.2.1 Design Approaches - There are a number of different approaches that can be used to design a seismic time history. Among the approaches, three good candidates are:

1. Use traditional seismic design procedures; ground motion developed from design response spectra – time history applied to a building – building motion applied to the pipe,
2. Design a "bounding" time history of excitation, and
3. Synthesize a time history from a floor response spectrum.

Consideration was given to using all three of these approaches in this effort before the third method was selected.

The first approach was the one that was used to design the IPIRG-2 seismic forcing function. In this approach, five basic steps were followed:

1. The NRC Regulatory Guide 1.60 ground acceleration response spectrum provided the basic description of the seismic input.
2. An artificial time-history of ground acceleration was generated that was spectrum-consistent with Step 1.
3. A simple model of a pressurized water reactor (PWR) plant was used as a transfer function between the time-history ground acceleration and an assumed location for the pipe system.
4. The relative motion between two "floors" in the PWR model and the inertial loading represented the loading to be applied to the pipe system.
5. The time-history of actuator motion for the pipe loop was defined by finding a displacement-time history that would give the same moment-time response at the crack location as the multi-point excitation defined in Step 4.

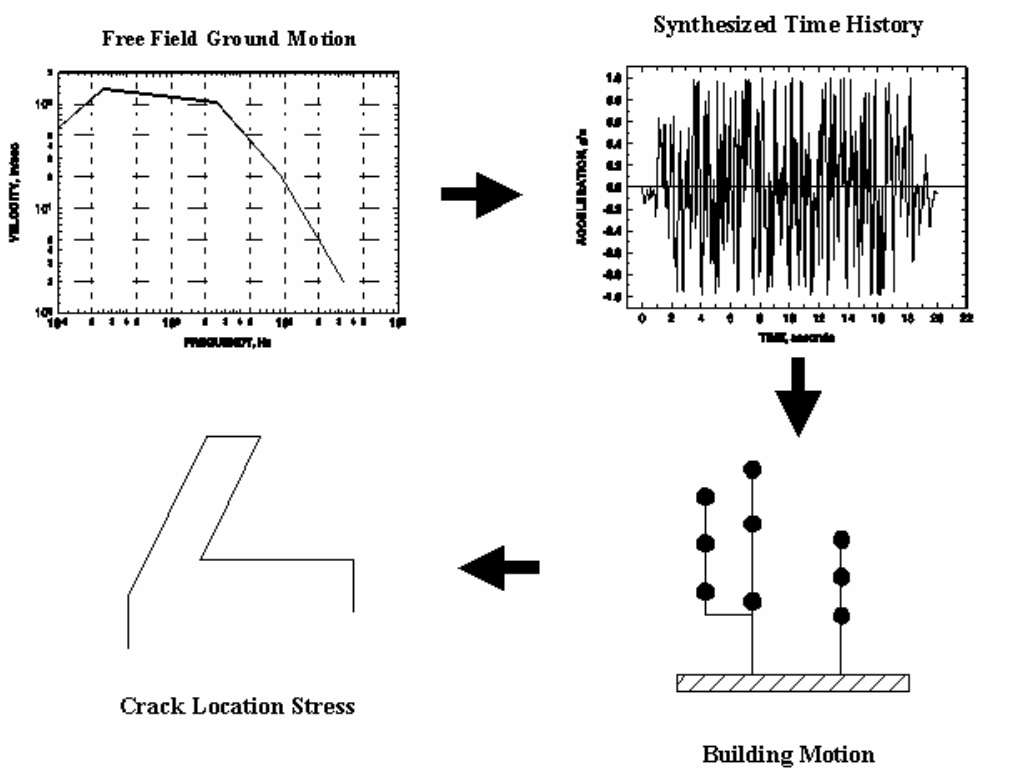

Figure B.3 Traditional seismic design process

Figure B.3 shows a pictorial representation of this seismic design process. This approach is not particularly difficult, but is quite tedious because many synthetic time histories must be considered. First, time histories must be qualified in terms of passing the seismic design rule prescriptions, and secondly, they must meet the BINP experiment requirements.

The second approach to designing a seismic time history was to use a "bounding" case type of loading. Based on the data available at the close of the IPIRG-2 program from C(T) specimen testing and the IPIRG pipe-system experiments, a worst case cyclic damage seismic time history was hypothesized to be as follows: single frequency excitation near the natural frequency of the pipe system, rise time of 3 to 5 seconds with increasing amplitude, strong motion duration of 4 to 15 seconds, and loading that makes the stress ratio less than -0.3 (i.e., significant compressive stresses at the crack location). Figure B.4 shows a conceptual idea of the "bounding case" forcing function. Assuming a 4 Hz natural frequency for a pipe system, 12 to 20 cycles of loading would occur in the build-up phase of the time history with 16 to 60 additional cycles that would continue to grow the crack after it has initiated. Such a time history would definitely invoke both cyclic and dynamic effects.

A third possible approach for designing the BINP seismic time history is to synthesize a time history from a floor response spectrum, see Figure B.5. This approach involves many of the same basic ideas as the first approach, but it is not quite as involved, given a target floor response. Unlike the second approach, this method has a solid foundation in seismic analysis techniques. It is, however, like the first approach, a trial and error process to find the right solution for the BINP program.

All three approaches for designing the BINP seismic time history were considered. The second method, the "bounding case" method, was very quickly dropped because it did not have enough of a seismic flavor. The first method, the IPIRG-2 design approach, was initially thought to be the best alternative since it already had good technical credentials. Unfortunately, the non-deterministic nature of the design process was judged to be a serious impediment. Regarding the last alternative, the floor response spectrum-based design, an IPIRG-2 Round Robin (Ref. B.2) conveniently was conducted on this very subject and thus, there was already a good body of basic data available for guiding the BINP seismic design. Because the round-robin results greatly simplified the design process, and because of the direct tie to the IPIRG-2 seismic forcing function, the floor-response spectrum analysis approach was selected for the BINP seismic forcing function design.

B.1.2.2 Material Property Issues - The test specimen to be used in the BINP simulated-seismic experiment was a nominal 16-inch diameter Schedule 100 TP304 stainless steel pipe, denoted as DP2-A8 in the Battelle material property library. This pipe has been used for a large number of the Degraded Piping Program and IPIRG experiments, and has been very well characterized in terms of stress-strain behavior and fracture toughness. Issues involved in the use of the TP304 base metal for the BINP test that have an impact on the seismic forcing function design include, which heat of TP304 is to be used in the experiment (high or low sulfur content) and which J-resistance behavior (quasi-static, dynamic, cyclic, monotonic) is most appropriate.

The pipe designated as A8 can have one of two different chemistries as documented in Reference B.3. Although both meet the TP304 specifications, eventually it was discovered in the IPIRG-2 program that the two different chemistries have very different fracture toughness levels, and different susceptibility to dynamic and cyclic loading effects, Figures B.6 and B.7. Not recognizing that all pipes delivered from the same lot and initially labeled as DP2-A8 are different can, in fact, disguise the role of cyclic and dynamic effects in pipe fracture experiments. Thus, it was important for the design of the BINP seismic forcing function to know which heat of TP304, A8i or A8ii, was going to be used in the experiment.

A second material property issue that impacts the design of the BINP seismic forcing function is the choice/selection of what kind of J-resistance curve to use: dynamic or quasi-static loading rates, at what stress ratio, and what cyclic plastic displacement. Clearly, the selection is based on the results of the pipe system stress analysis, which in turn is based on the selection of the J-resistance curve, i.e., it is a circular proposition.

The decision about A8i and A8ii was easily resolved by a chemical analysis, i.e., the BINP test specimen was from heat A8ii (the higher sulfur content, lower toughness heat). Likewise, the decision about whether to use dynamic or quasi-static data was quite easy, because the loading is dynamic. The appropriate stress ratio and cyclic plastic displacement increment to use was an iterative process driven by the dynamics and scaling of the forcing function.

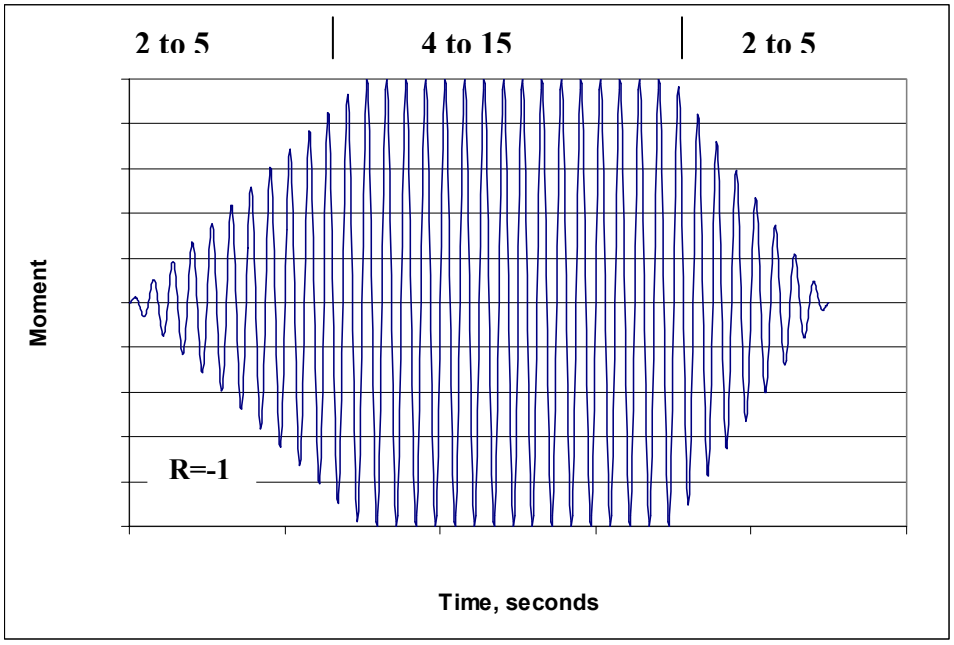

Figure B.4 Hypothesized worst case seismic loading

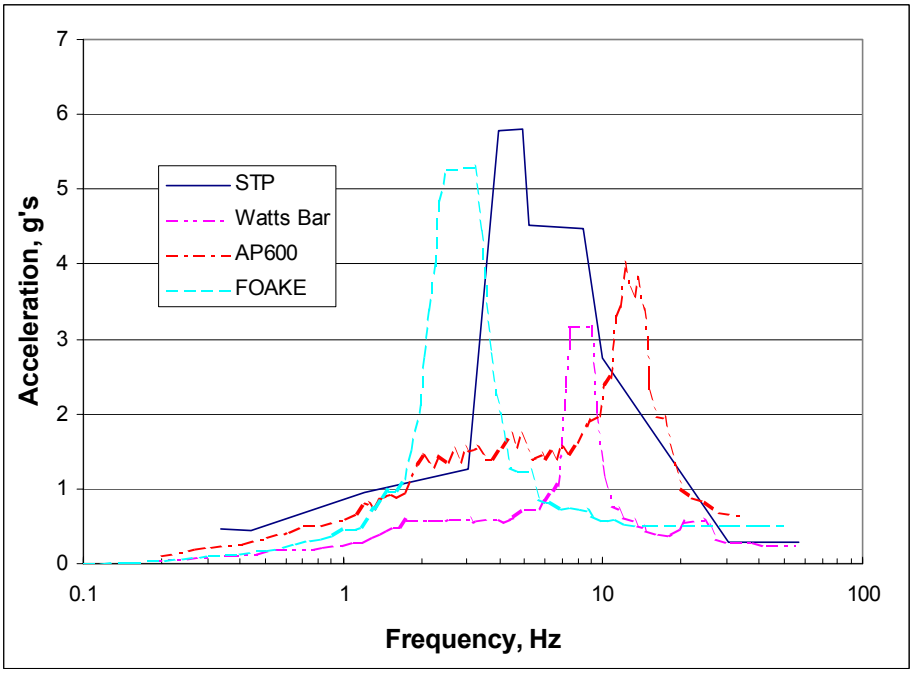

Figure B.5 Typical SSE seismic floor-response spectra

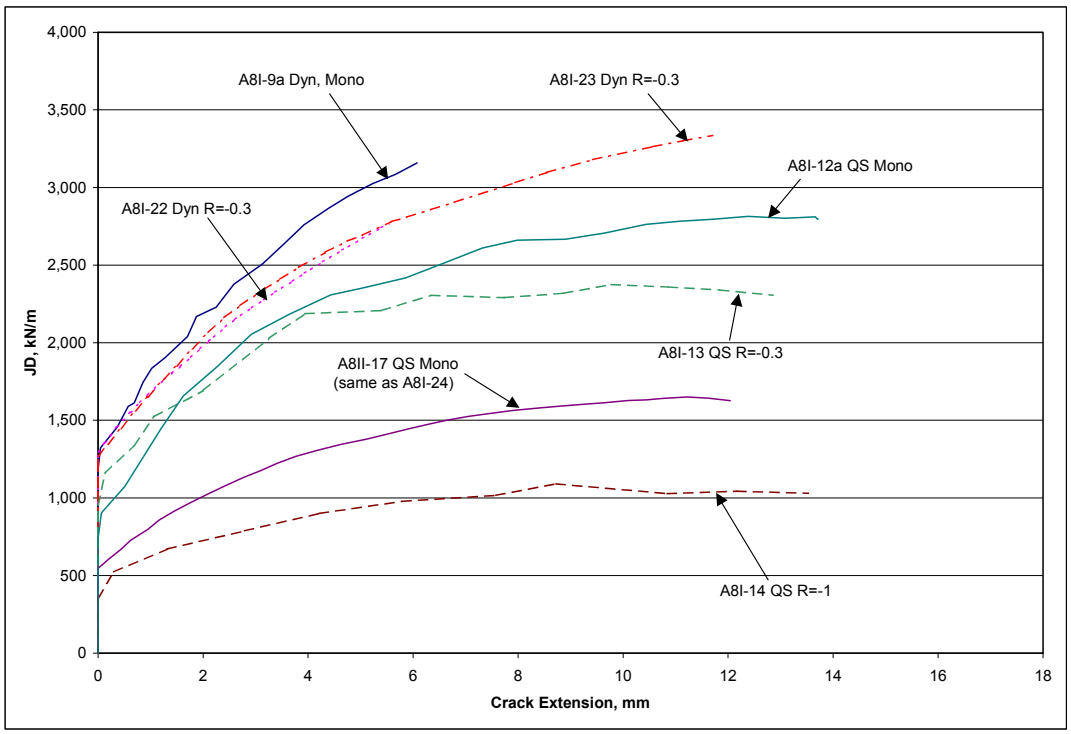

Figure B.6 Fracture toughness properties from pipe DP2-A8i

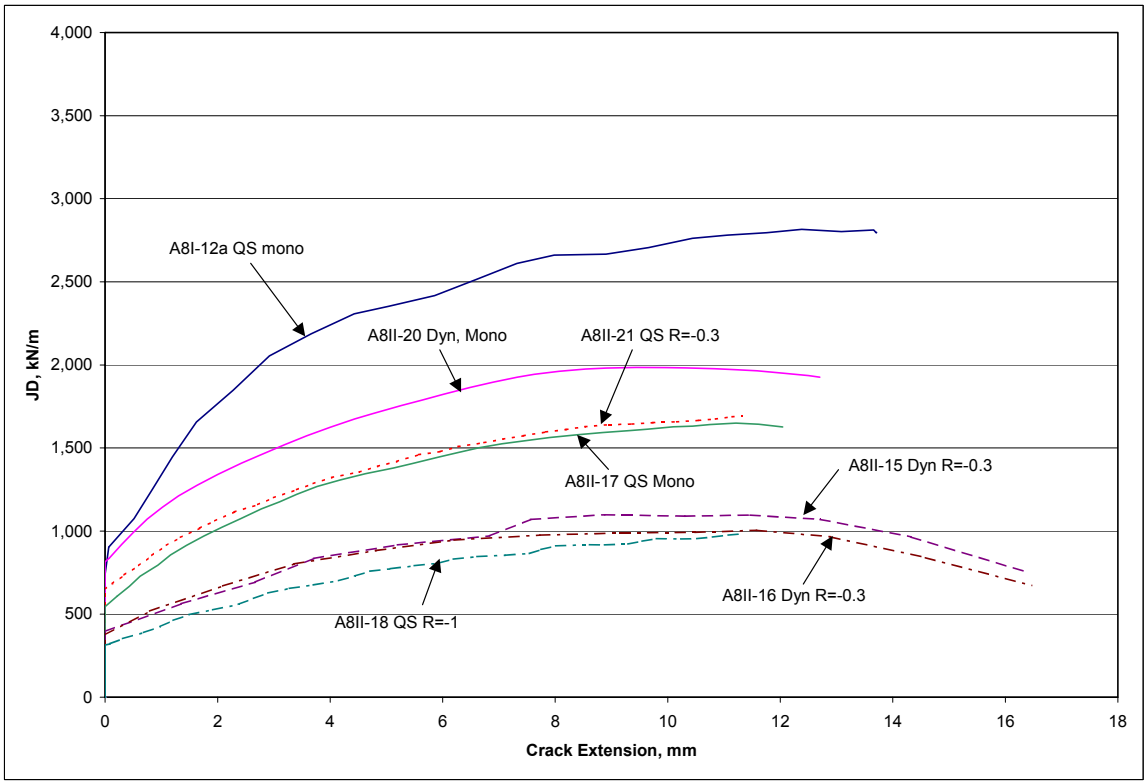

Figure B.7 Fracture toughness properties from pipe DP2-A8ii

B.1.2.3 ANSYS Implementation Issues - In all of the design exercises for the IPIRG pipe-system experiments, dynamic, nonlinear spring, time-history finite element analysis have been successfully used with analysis tools that have evolved to a fairly sophisticated level, Ref. B.4. In these previous analyses, the best available data have been used to define the crack nonlinear response – quasi-static pipe tests at first, moving to J-estimation scheme analyses with quasi-static J-R curves and stress-strain data, and finally ending with J-estimation scheme analyses with dynamic J-R curves.

The nonlinear crack behavior in the finite element analyses has been characterized as crack moment versus crack rotation and, for surface cracks, has been implemented as a set of three elastic-perfectly plastic springs in parallel, see Figure B.8. Implicit with the nonlinear spring formulation is the assumption of kinematic hardening, i.e., yielding in the compressive direction occurs at $2\sigma_y$ below a plastic unloading point, Figure B.9. This is equivalent to saying that the compressive moment-rotation response is the mirror image of the tension moment-rotation response. Furthermore, because the nonlinear behavior of the crack is modeled only as moment-rotation, effects such as axial loading, which affects the state of stress at the crack tip, must be "built into" the moment-rotation curve. That is, a crack with pressure and moment loading will have an apparently lower moment-rotation resistance than a crack with moment only loading, Figure B.10.

Historically, all of the analyses for the IPIRG-1 and IPIRG-2 programs have been conducted with moment-rotation curves developed for moment plus pressure loading. Intuitively, this would seem to be the correct thing to do and, for cases where the unloading is limited, i.e., most of the IPIRG single frequency loading experiments, it is quite reasonable. However, for cases where significant reverse loading is expected, i.e., seismic loading, compressive yielding will occur far too early if a pressure-corrected moment rotation curve is used.

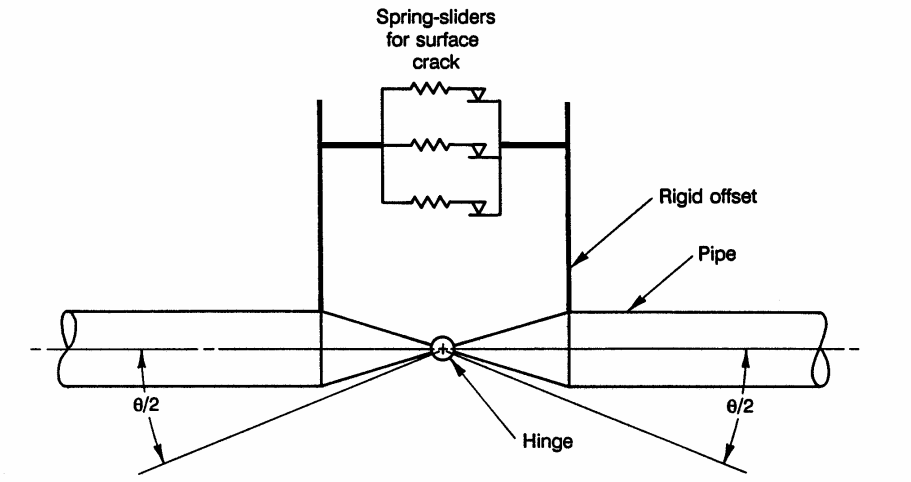

Figure B.8 Spring-slider model for a surface crack

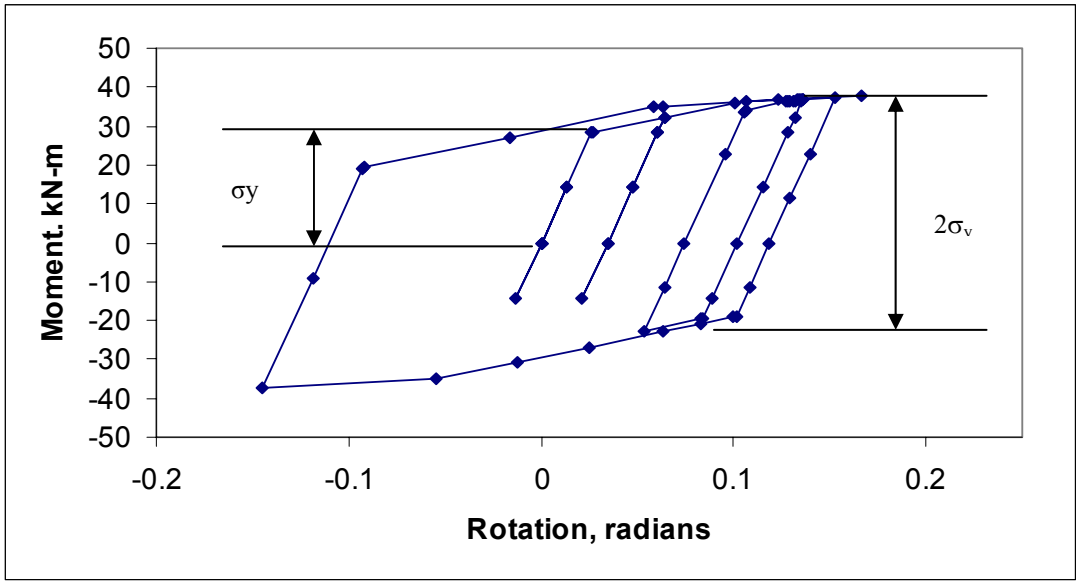

Figure B.9 Kinematic hardening assumption under unloading conditions

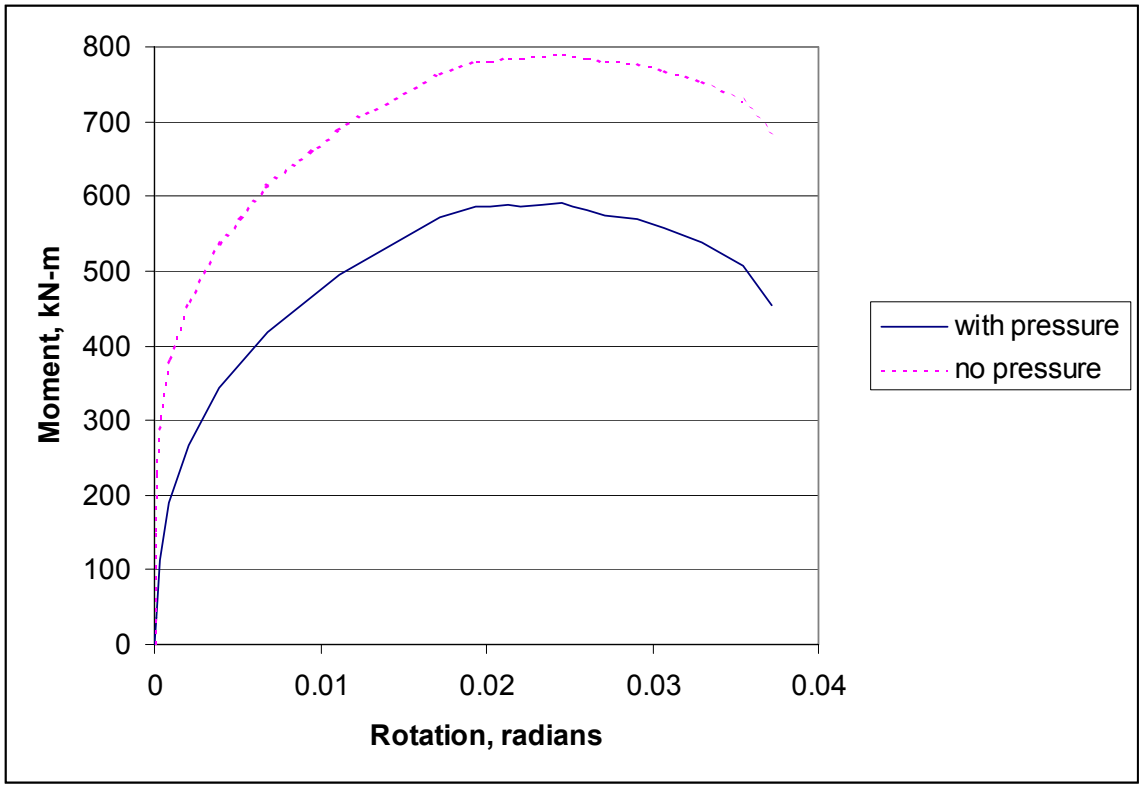

Figure B.10 The effect of pressure on crack moment-rotation behavior (BINP Task 2 flaw, A8ii-20 dynamic monotonic J-resistance)

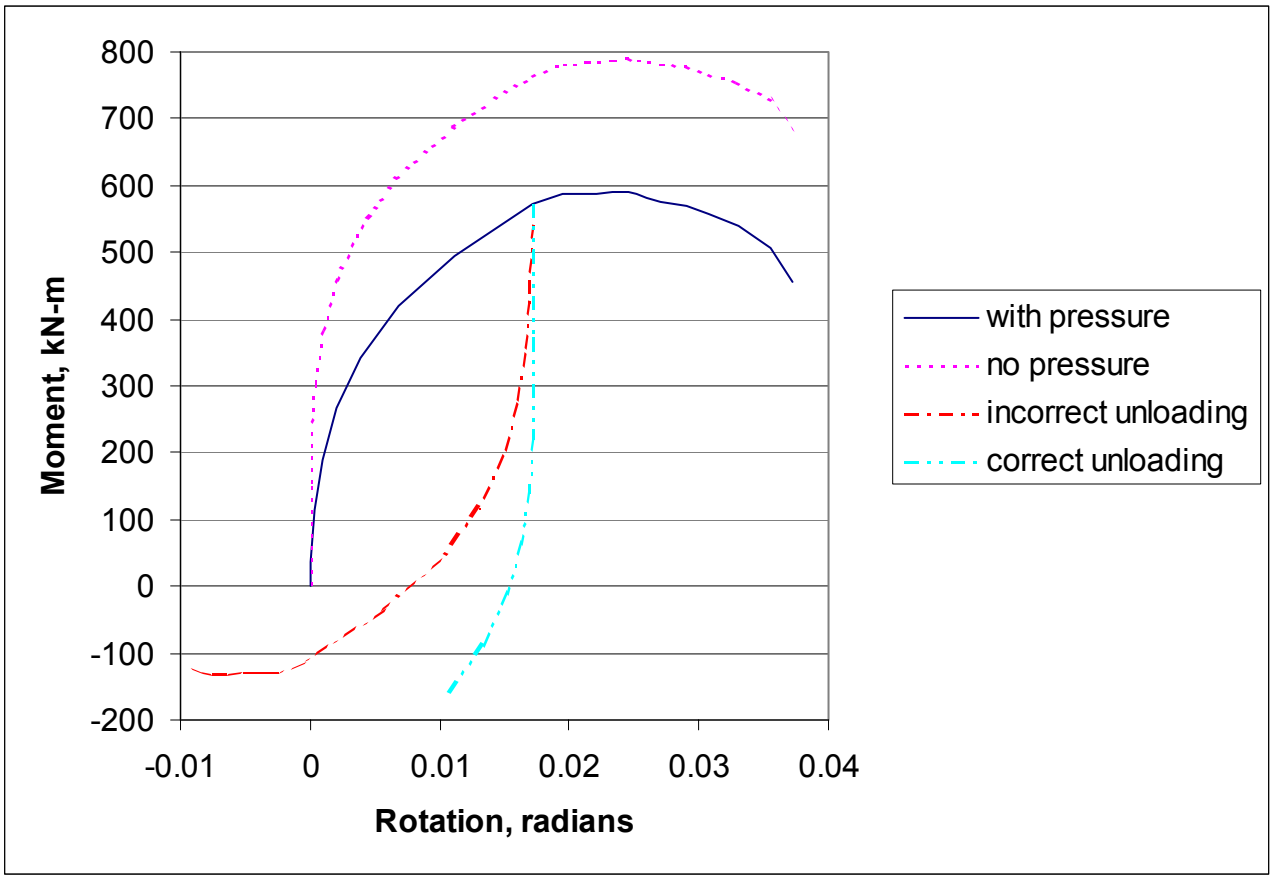

Figure B.11 Crack unloading behavior

Basically, because the pressure-corrected moment-rotation curve is the mirror image of the tensile moment-rotation curve, it is as if the stress at the crack tip, caused by pressure, changes sign when the crack is unloaded, a totally inappropriate response. The crack should unload elastically much further before it yields in compression, Figure B.11. This is quite important for the design of a seismic forcing function because it is the unloading that determines the stress ratio and hence, the amount of cyclic degradation that will occur. Like the fact that the IPIRG-2 seismic loading was not very challenging, this crack modeling deficiency was not recognized until the close of the IPIRG-2 program. Overcoming this deficiency in the unloading behavior of the nonlinear spring model requires that a slightly different approach be used to model the nonlinear behavior of cracks.

Any new modeling approach for surface cracks loaded with pressure and bending to better define the compressive loading behavior needs to include the following:

- Tensile loading failure based on pressure plus bending,
- Consistency with kinematic hardening rules, i.e., $2\sigma_y$ yielding behavior, and
- Compressive loading to account for the pressure effect.

Taken as a whole, these conditions imply that the moment-rotation response of the crack must be asymmetric, i.e., compression is not a mirror image of tension. The last two conditions imply that compressive yielding in moment-rotation coordinates must occur at twice the tensile yield moment (including the pressure effect) plus twice the pressure-induced moment effect.

Figure B.11 provides a pictorial representation of the desired behavior.

Implementation of asymmetry in the moment-rotation response in the finite element model would, in general, require a special constitutive model or a special element that ANSYS does not have in its standard element library. The desired response, however, can be achieved with the current elements as follows:

1. Define the expected tensile crack moment-rotation behavior using a J-estimation scheme analysis that includes pressure,
2. Define the pressure contribution to the tensile failure by running a J-estimation scheme analysis identical to the first one, but without pressure,
3. Use the data from the second analysis to define the "springs" and "sliders" for the nonlinear crack model,
4. Apply + and - crack opening moments at the two nodes of the spring-sliders equal to the moment difference between the results from Step 1 and Step 2, and
5. Conduct the analysis as usual.

The net effect of this process is to make the crack moment-rotation response appear asymmetric as far as tensile and compressive yielding of the crack is concerned. However, as far as the pipe system is concerned, everything is as it should be:

- The stresses in the pipe will be calculated correctly because the moments applied in Step 4 sum to zero.
- The incremental tensile moment that the crack can stand will be correct because the moments applied in Step 4 make up the difference between the moments the spring sliders in the model will permit and the real failure moment calculated in Step 1.

Validation Analyses - To provide some level of comfort that the new surface crack modeling approach is rational, an analysis of IPIRG-2 Experiment 1-1 was conducted to see how well the analysis compares with an experiment. (Experiment 1-1 is the "companion" IPIRG-2 seismic loading experiment to the present BINP experiment.) Figures B.12 and B.13 show the measured pipe response from the experiment up to surface-crack penetration.

IPIRG-2 Experiment 1-1 used Battelle pipe DP2-A8i. (Note: this is not the same material as used in the BINP experiment.) Available J-resistance curve data for DP2-A8i include quasi-static data (A8i-12a: monotonic, A8i-13: R = -0.3, A8i-14: R = -1.0), and dynamic data (A8i-9a: monotonic, A8i-22 and A8i-23: R = -0.3, A8i-24: R = -1.0). Stress-strain data at a variety of testing rates are also available, although no significant rate dependence has been observed for either DP2-A8i or DP2-A8ii. Obviously, the dynamic J-R data are most appropriate for this analysis.

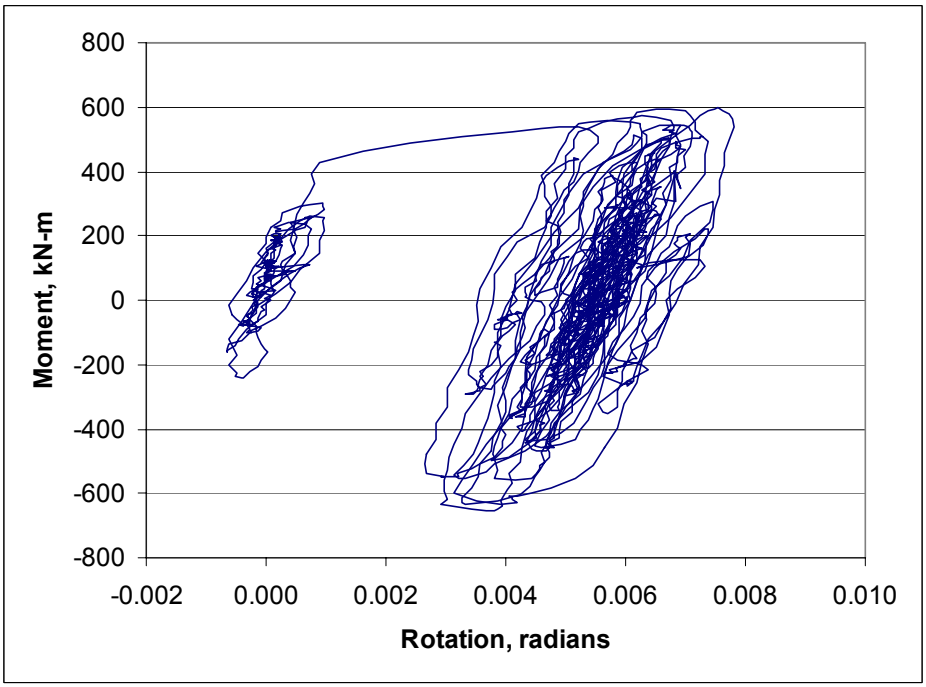

Figure B.12 IPIRG-2 Experiment 1-1 cracked-section moment-rotation response

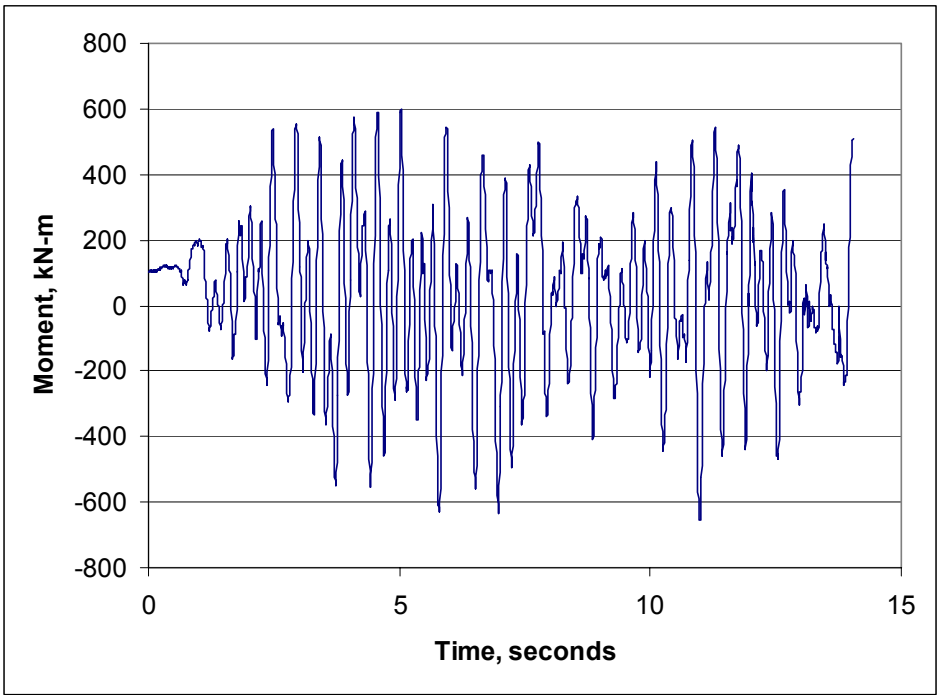

Figure B.13 IPIRG-2 Experiment 1-1 cracked-section moment-time history

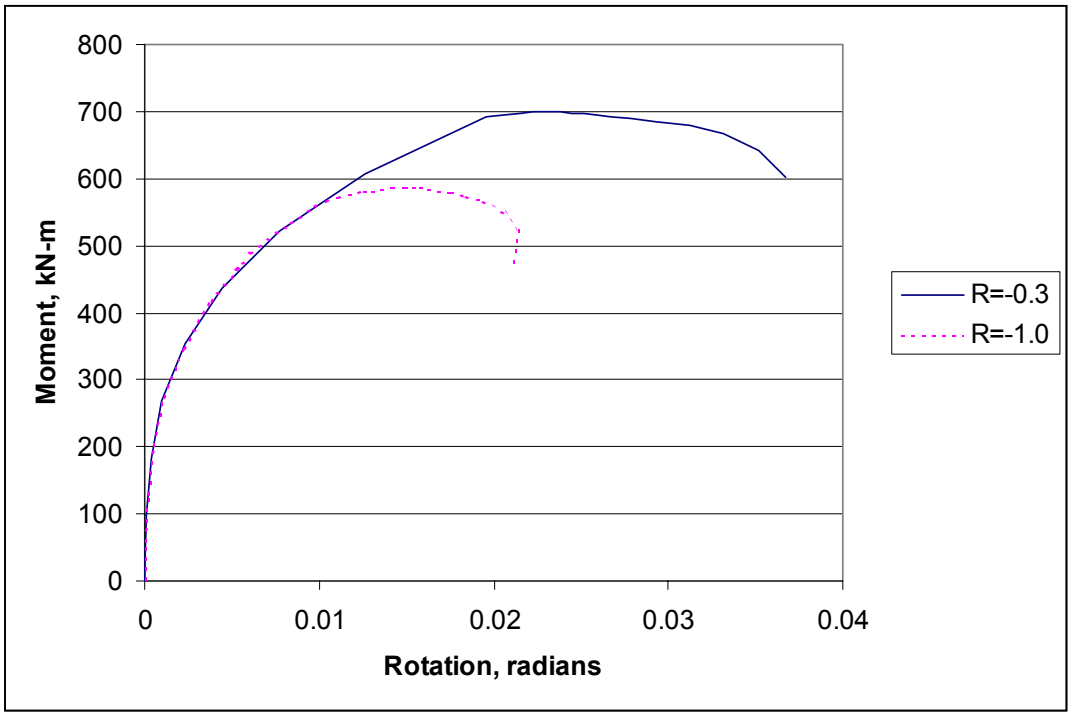

Figure B.14 IPIRG-2 Experiment 1-1 predicted cracked-section upper envelop moment-rotation from the SC.TNP1 J-estimation scheme

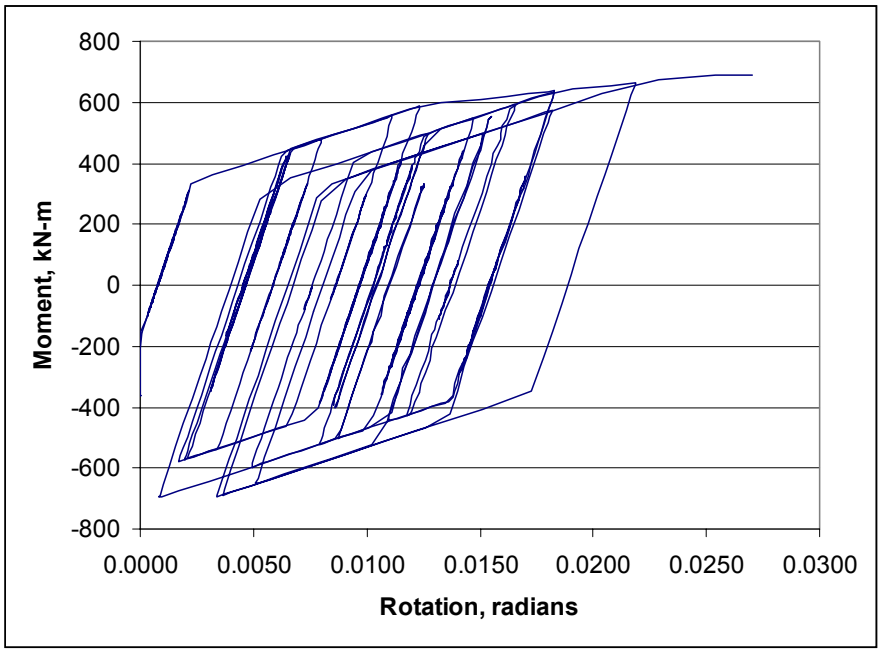

Figure B.15 Predicted IPIRG-2 Experiment 1-1 moment-rotation history using the dynamic R = -0.3 J-R curve with the new asymmetric moment-rotation model

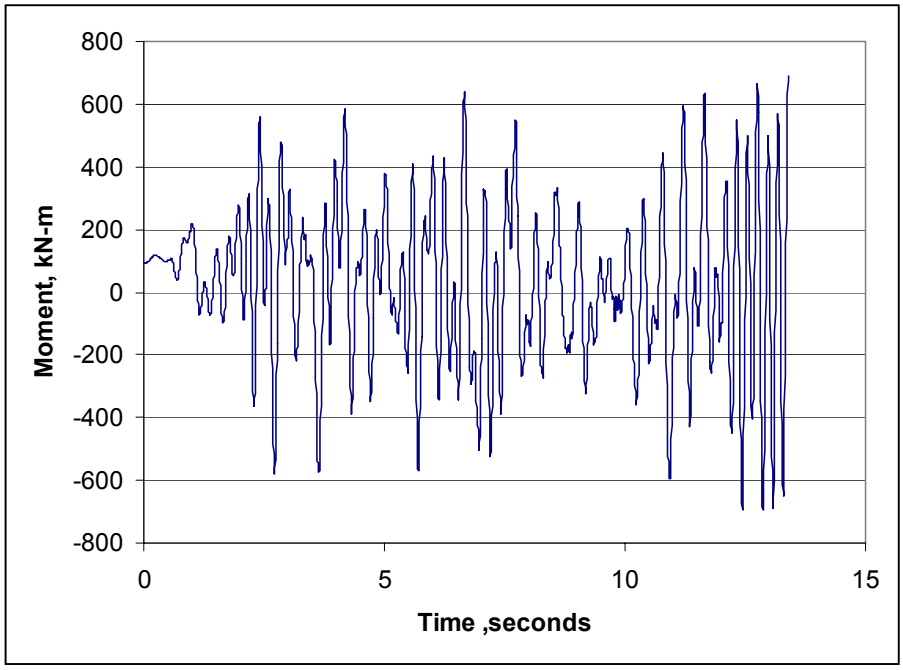

Figure B.16 Predicted IPIRG-2 Experiment 1-1 moment-time history with the dynamic R = -0.3 J-R curve with the new asymmetric moment-rotation model

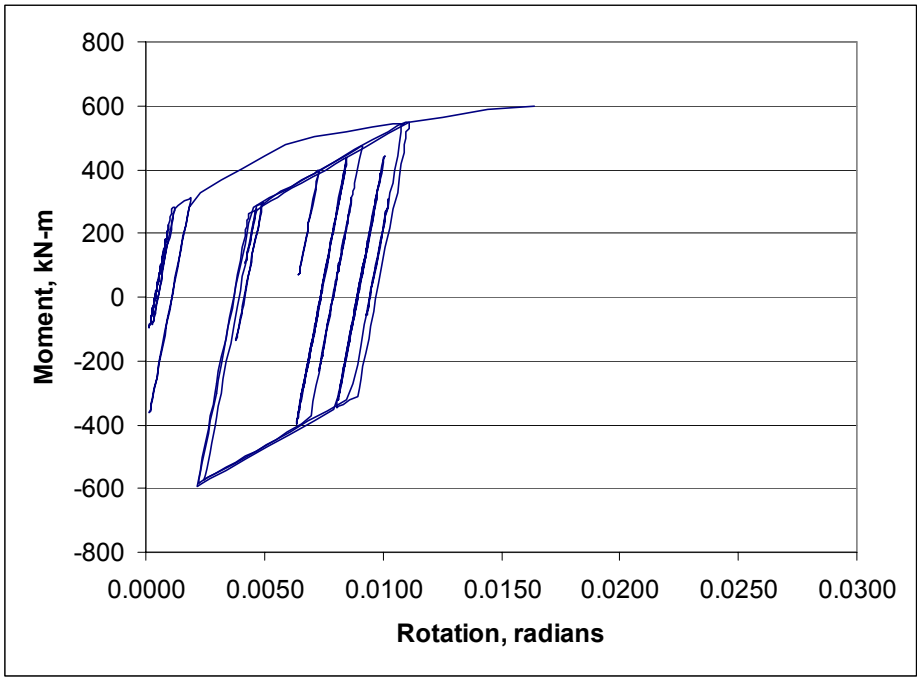

Figure B.17 Predicted IPIRG-2 Experiment 1-1 moment-rotation history with the dynamic R = -1.0 J-R curve with the new asymmetric moment-rotation model

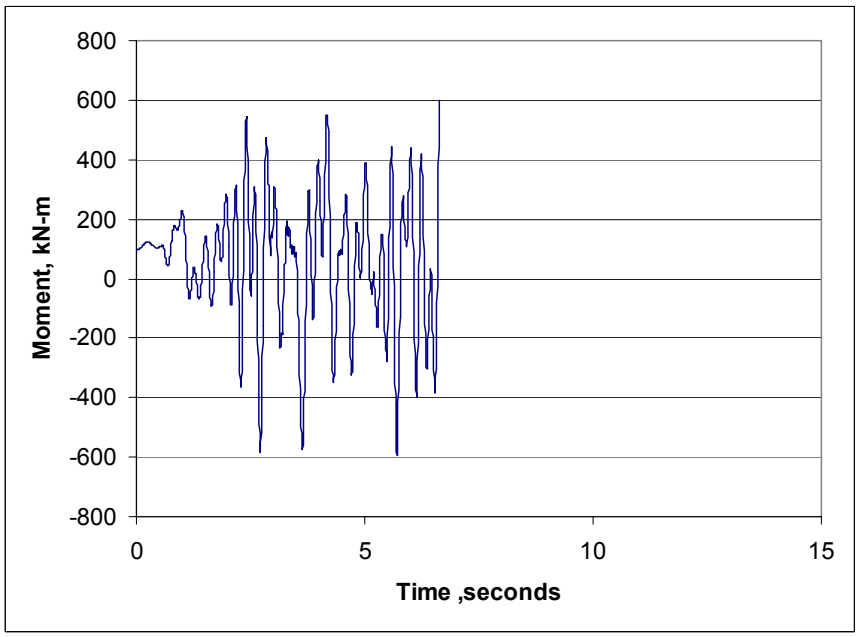

Figure B.18 Predicted IPIRG-2 Experiment 1-1 moment-time history with the dynamic R = -1.0 J-R curve with the new asymmetric moment-rotation model

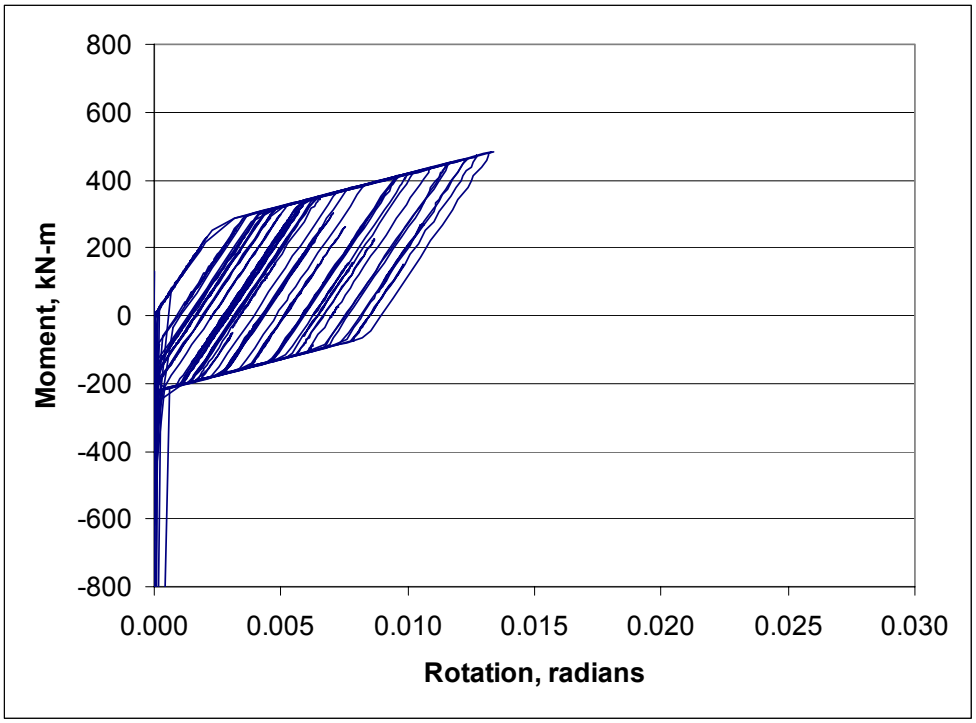

Figure B.19 Old (1993) IPIRG-2 Experiment 1-1 pretest design analysis moment-rotation history results

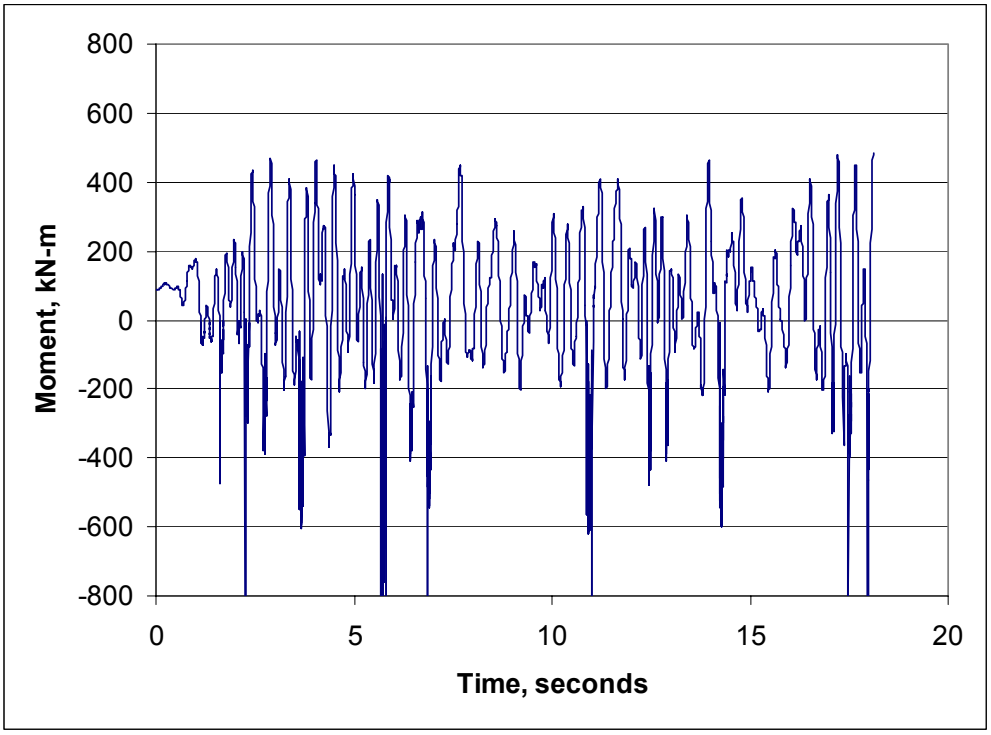

Figure B.20 Old (1993) IPIRG-2 Experiment 1-1 pretest design analysis moment-time results

The result of any analysis is driven by the selection of the moment-rotation response. This, in turn, is a function of the J-R curve, which is a function of the stress ratio and plastic displacement increments. In general, the stress ratio and plastic increments are not known until an analysis has been completed. In this case, however, because the results of the experiment are available, the "best" J-R curve can be immediately selected. Inspection of the experimental results of Experiment 1-1 suggests that the effective stress ratio (a function of the actual stress ratio and plastic increments) varies between R = -0.3 and R = -0.6. To bound the expected behavior, analyses were conducted using moment-rotation curves developed from J-R curves for R = -0.3 and R = -1.0.

The predicted moment-rotation behavior for the IPIRG-2 Experiment 1-1, generated using the SC.TNP1 analysis in NRCPIPES Version 3.0, is shown in Figure B.14.

Using the design seismic forcing function (there is virtually no difference between the designed function and the experimentally measured actuator response), ANSYS nonlinear-spring analyses were conducted to the point of maximum load, i.e., presumed surface-crack penetration, using the new compressive unloading behavior model. Figures B.15 through B.18 show the results of the "bounding" analyses. For reference, Figures B.19 and B.20 show the results of the IPIRG-2 Experiment 1-1 pretest analysis that used the mirror image of the bending plus tension moment-rotation response in the compressive regime.

For these curves, the equivalent crack length (measured crack area divided by the measured maximum crack depth) was used. There are significant differences between these curves because at R = -0.3, there is very little degradation from the monotonic case, whereas at R = -1.0, the J-R curve, and hence moment-rotation is significantly affected.

Comparing Figures B.12, B.15, B.17, and B.19, qualitatively, the new analyses are much closer to the experiment than the "old" analysis in two

regards: 1) the new analyses do not show the severe crack closures that the old analysis did, and 2) the new analyses show evidence of the large monotonic load cycle that the old analysis did not predict. Quantitatively, the new analyses bracket the experimentally observed failure moment, whereas the old analysis is low, although there is a good reason for this – the old analysis was a pretest prediction that used the best pretest estimate of the flaw size, whereas the new analyses used the measured flaw size. Quantitatively, it is also important to note that the rotations in the new analyses are very much larger than the experimentally observed rotations. This is a J-estimation scheme problem – the ANSYS nonlinear spring analysis is only as good as the input from the J-estimation scheme. As a final observation, in the experiment, surface-crack penetration occurred long after maximum moment.

Within the bounds of the ANSYS nonlinear spring analysis, this just cannot be predicted because surface-crack penetration is defined to happen at maximum moment. From an experimental perspective, what this implies is that there was either cyclic or fatigue damage that contributed to the eventual failure.

In general, the new analysis appears to be an improvement upon the previous method. The crack closures that are a part of the old technique would profoundly bias a seismic design analysis because it would suggest that the stress ratio was much more negative than it really is. Since stress ratio is one of the principal governing factors in cyclic damage, it is important to calculate it correctly. The new analysis technique, although not perfect, is a distinct improvement over the old technique and should lead to a better design for the BINP simulated-seismic experiment.

B.1.3 Design Details for the Simulated-Seismic Forcing Function

B.1.3.1 Design Process - The BINP seismic forcing function design process, as noted earlier, was based on developing a time history from a floor-response spectrum. In particular, the design was based on the results of IPIRG-2 Round-Robin Problem C.1, "Spectrum-Compatible Time-Histories". In this round robin, the participants were given a peak-broadened IPIRG-2 SSE actuator acceleration response spectrum at 2-percent damping, Figure B.21, and were asked to provide a spectrum-compatible displacement-time history of actuator motion. The resulting motion was then applied to a linear elastic finite element model of the IPIRG pipe loop by Battelle to see the effect of different "equivalent" time histories on applied crack bending moment.

Four solutions to the round-robin problem were submitted and all solutions were based on the same methodology: acceleration was assumed to be the sum of a number of sine functions with variable amplitudes and random phase angles, sine amplitudes were fixed using an iterative process, "raw" accelerations were somehow filtered to meet target maximum displacement prescriptions.

The key feature of this round-robin problem that led it to be considered for the design of the BINP seismic forcing function was that two of the submitted solutions, F-3a and D, show a nice build-up of moment at the early part of the solutions for linear analysis, Figures B.22 and B.23. Figures B.24 and B.25 show the corresponding actuator time histories from Solutions F-3a and D at an SSE scaled level. Given the two candidate time histories of actuator motion, the BINP seismic forcing function design process reduced to finding the best scaling and "tuning" factors for one of the histories so that it would meet the BINP seismic forcing function design goals. As suggested earlier, the scaling and tuning process is iterative, involving a significant number of nonlinear analyses. The guiding principles for the design were a desire to have significant cyclic degradation (stress ratio at or below R=-0.3, see Figure B.25), a desire to have gradual build-up of stress amplitude with about 10 plastic displacement (rotation) cycles, and a desire to have failure occur in the range of 5 to 10 seconds.

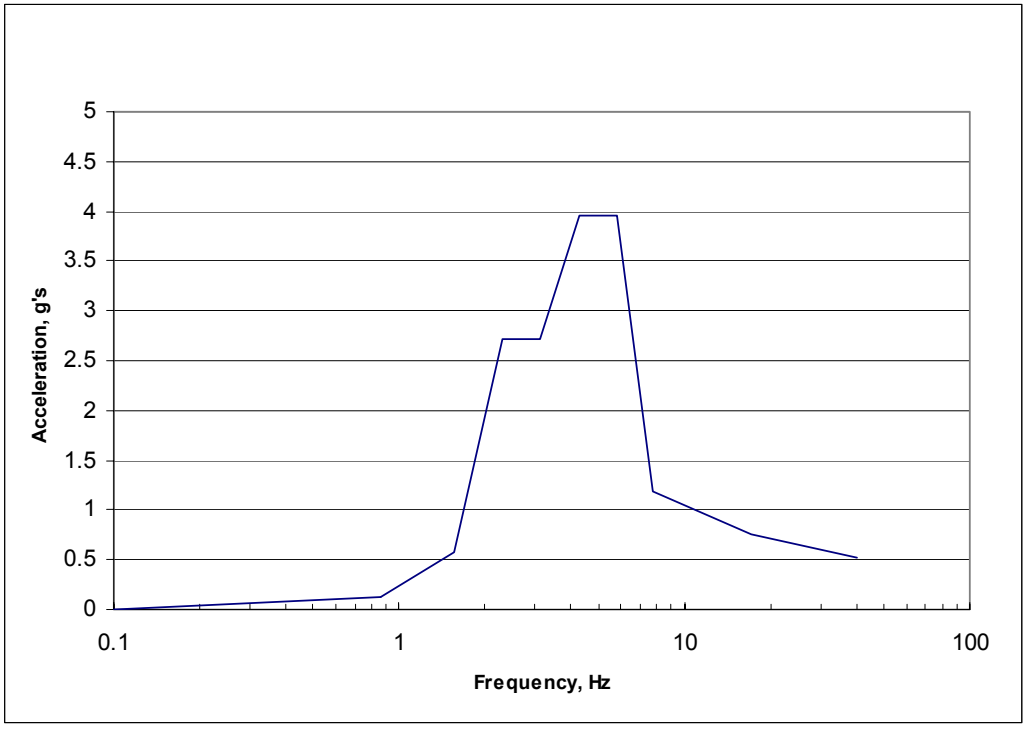

Figure B.21 The IPIRG-2 Round-Robin Problem C.1 floor-response spectrum (IPIRG-2 simulated-seismic forcing function actuator acceleration at SSE loading)

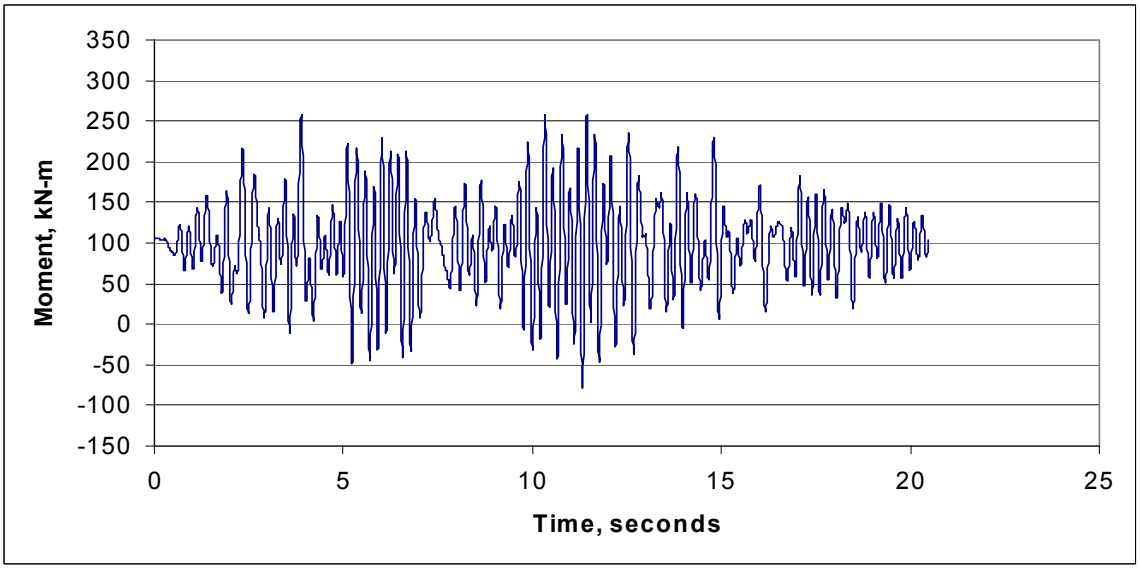

Figure B.22 IPIRG-2 Round-Robin Problem C.1 predicted linear moment response from Solution F-3a

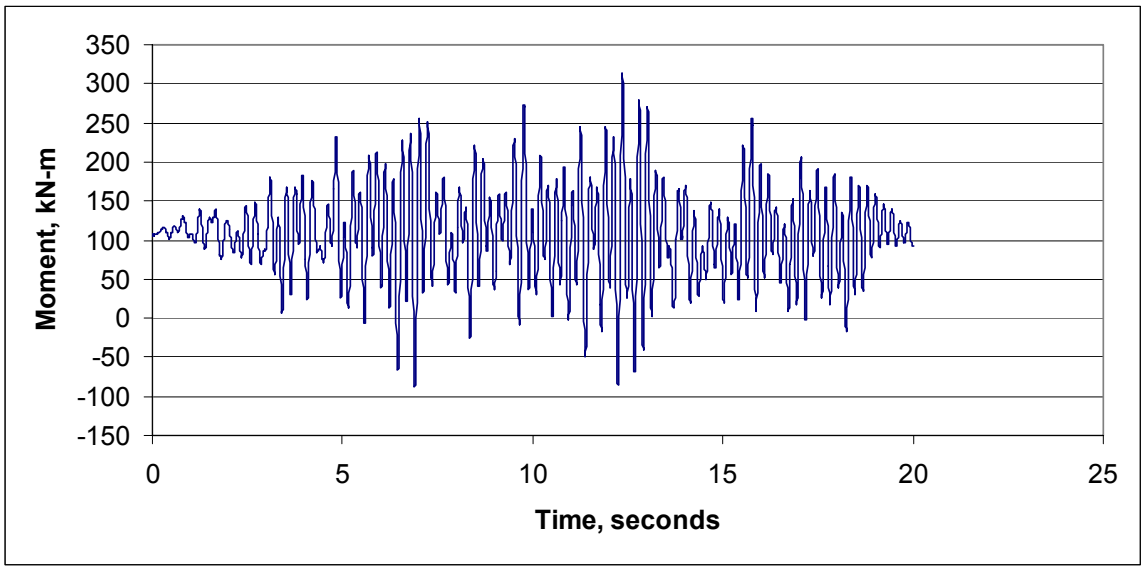

Figure B.23 IPIRG-2 Round-Robin Problem C.1 predicted linear moment response from Solution D

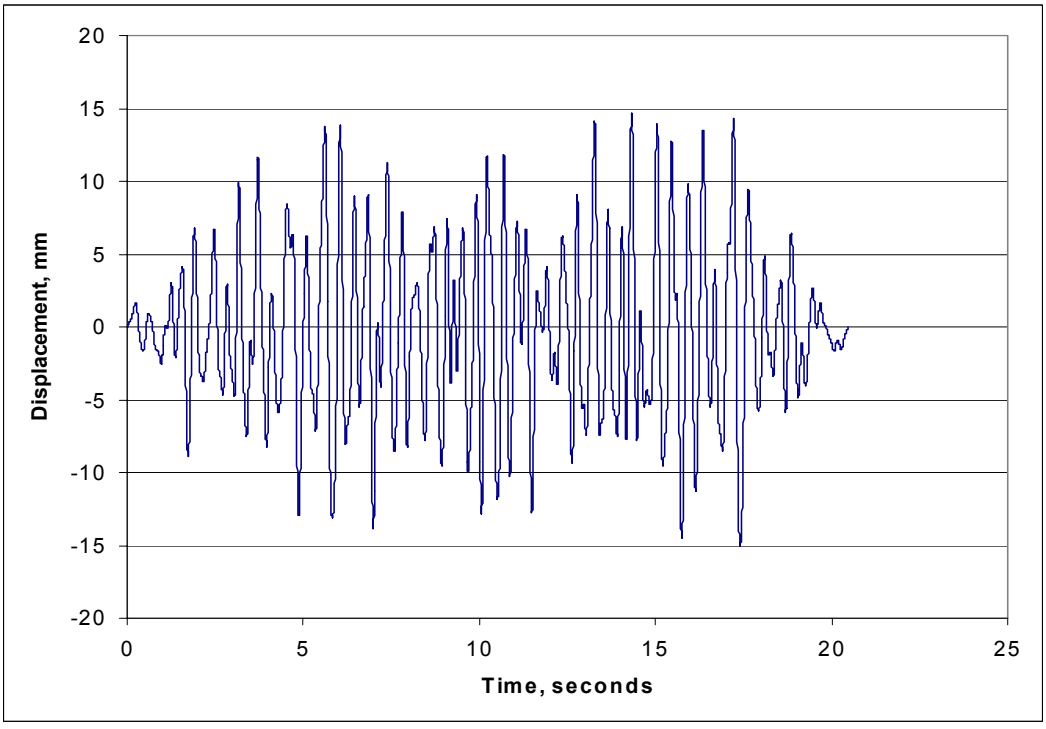

Figure B.24 IPIRG-2 Round-Robin Problem C.1 Solution F-3a actuator displacement forcing function

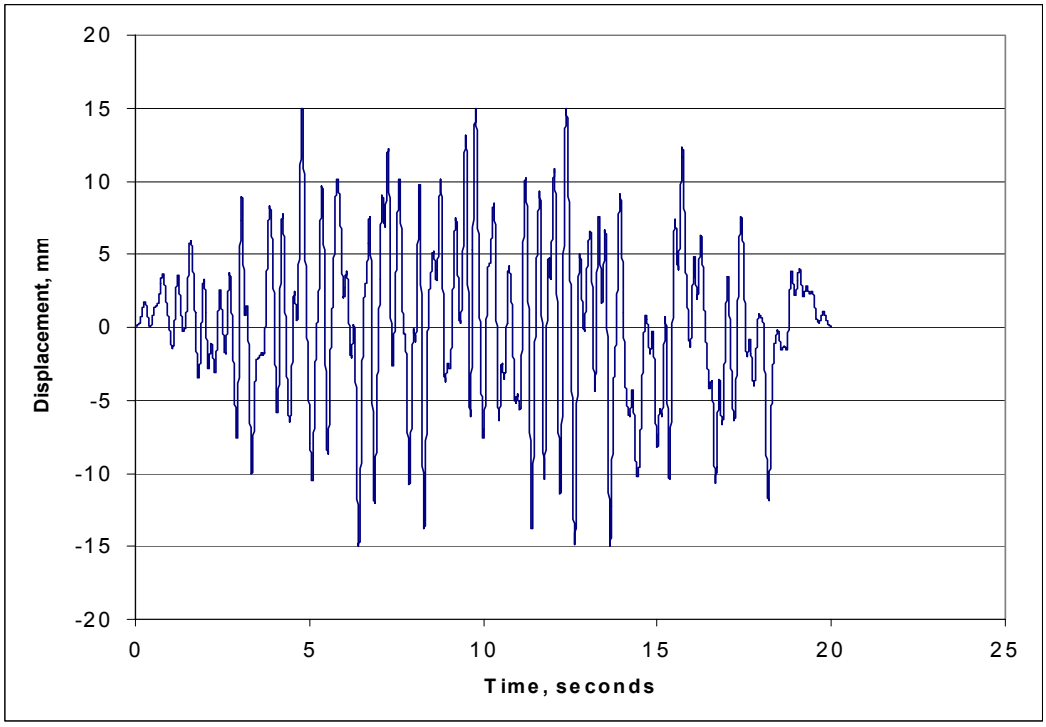

Figure B.25 IPIRG-2 Round-Robin Problem C.1 Solution D actuator displacement forcing function

The predicted pipe-system response is a function of the moment-rotation curve used in the analysis. It is expected that the BINP Task 2 crack will behave according to the response dictated by the dynamic, R = -0.3 J-resistance curve. In the extreme, however, the behavior might be as good as if the pipe had quasi-static, R = -0.3 J-resistance properties. Figure B.26 shows the expected extremes in moment-rotation behavior for the experiment calculated using the SC.TNP1 analysis in NRCPIPES Version 3.0 using the A8ii-15 (dynamic, R = -0.3) and A8ii-21 (quasi-static, R = -0.3) J-R curves. [Note: the cyclic J-R curves had a ratio of cyclic plastic displacement to monotonic plastic displacement at crack initiation of 0.1. That is, 10 plastic displacement cycles were required before crack initiation.] For reference, the dynamic monotonic behavior is also shown. To be certain that the chosen forcing function will be able to fail the pipe in a single loading, it was decided that it would be good if the selected forcing function was able to fail cracks with either dynamic or quasi-static, R = -0.3 J-R curve behavior.

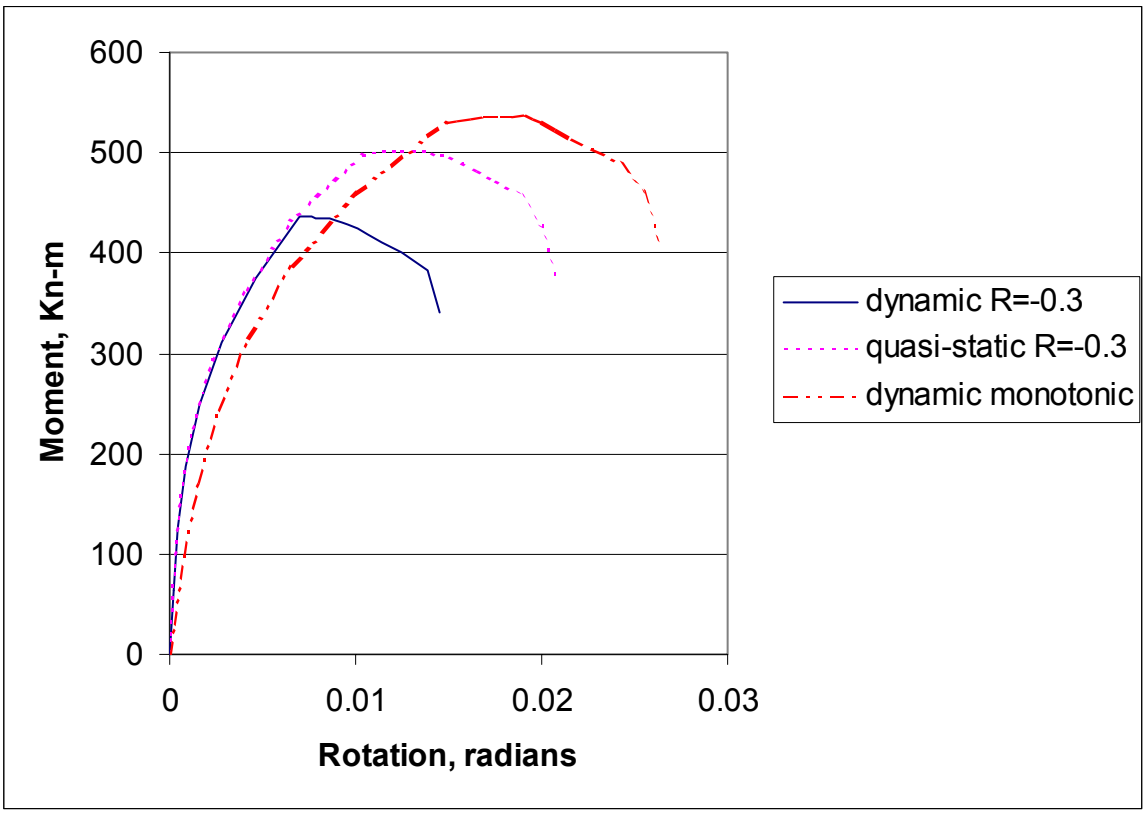

Figure B.26 BINP Task 2 predicted cracked-section upper envelop moment-rotation from the SC.TNP1 J-estimation scheme

B.1.3.2 Selection and Scaling - Initially it was felt that the F-3a solution was the most promising. However, subsequently it was discovered that nonlinear behavior at 4 SSE, at least with dynamic monotonic crack behavior, substantially modifies the Solution F-3a response. Fundamentally, the nonlinear crack acts like damping, phase shifting the system response. Initial analysis with Solution D using dynamic monotonic crack behavior at 4 SSE looked very promising, so a process of scaling and "tuning" the Solution D forcing function was undertaken.

Scaling and "tuning" of the Solution D forcing function to eventually settle on the BINP forcing function involved three inter-related processes:

1. Changing of the initial static actuator offset to decrease the stress ratio,
2. Scaling the amplitude of the SSE level forcing function up so that maximum moment is achieved, and
3. Modifying one of the displacement peaks in the original forcing function to get a better amplitude build up.

This process is an iterative one involving a significant number of nonlinear pipe-system analyses. The new surface-crack analysis methodology (asymmetric tension and compression), as described in Section B.1.2.3, is necessary for these analyses.

Figures B.27 through B.30 show the final results of analyses with the scaled and "tuned" Round-Robin Solution D forcing function with the BINP Task 2 bounding case crack moment-rotation curves. Figure B.31 shows the forcing function used to generate these results. For

either moment-rotation response assumption, the forcing function meets all of the BINP seismic forcing function design goals:

- Significant cyclic damage potential (the stress ratio (R) is between – 0.3 and – 1.0),
- 5 to 10 plastic cycles (there are 7 or 9), and
- Reasonable time to failure (it is 6.775 or 9.770 seconds).

The scaling and "tuning" amounted to scaling the basic Round-Robin Solution D up by a factor of 3, limiting the amplitude of the large actuator displacement at time 4.790 seconds to 8.89 mm (0.35 inch) [it was 15.01 mm (0.591 inch)], and offsetting the actuator by -12.7 mm (0.5 inch) at the start of the test. The scaling up is necessary to get a failure. (In the light of the IPIRG simulated-seismic test results from the SSE loading, it would be very surprising if SSE loading would cause a failure). Reducing the large amplitude has no dramatic effect on the response spectrum of the actuator motion, but it improves the cyclic moment build up. Offsetting the actuator reduces the initial bending moment caused by thermal expansion and makes the stress ratio more negative. Relating this actuator offset to real plant operations, it merely means that the expansion loop is more effective in controlling thermal expansion stresses.

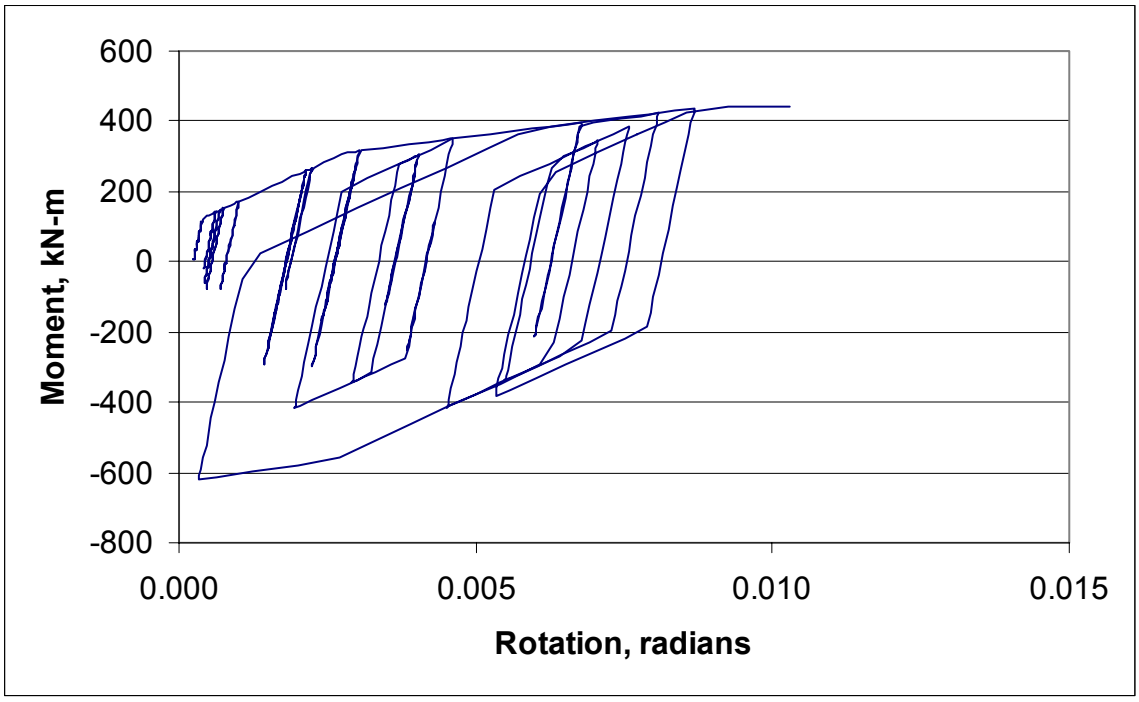

Figure B.27 Predicted BINP Task 2 cracked-section moment-rotation behavior using the dynamic R = -0.3 J-R curve

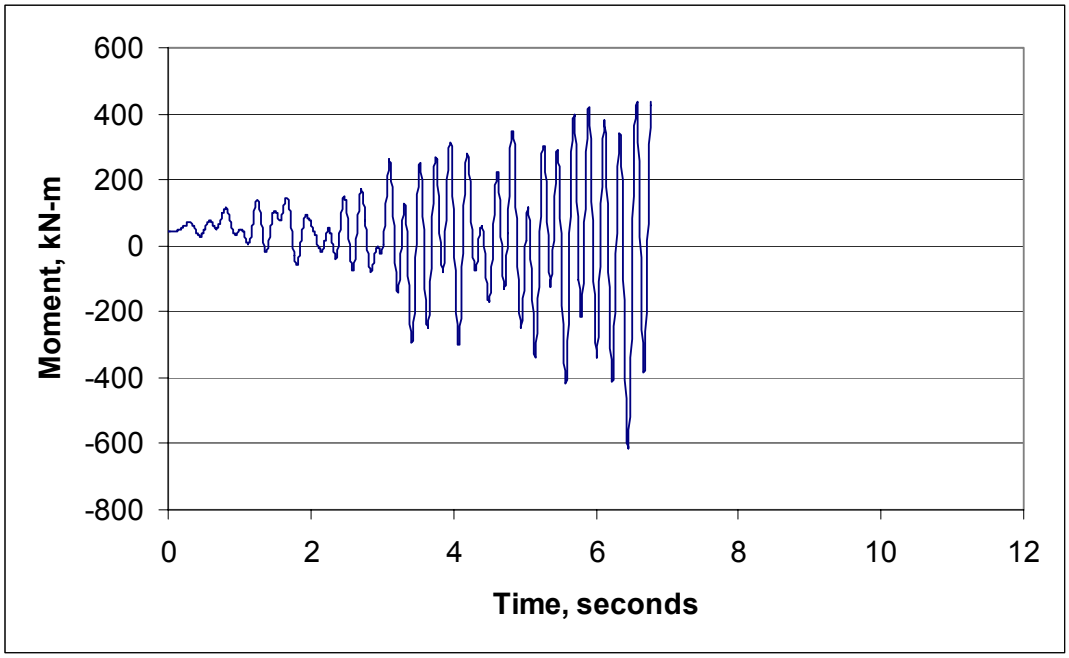

Figure B.28 Predicted BINP Task 2 moment-time behavior using the dynamic R = -0.3 J-R curve

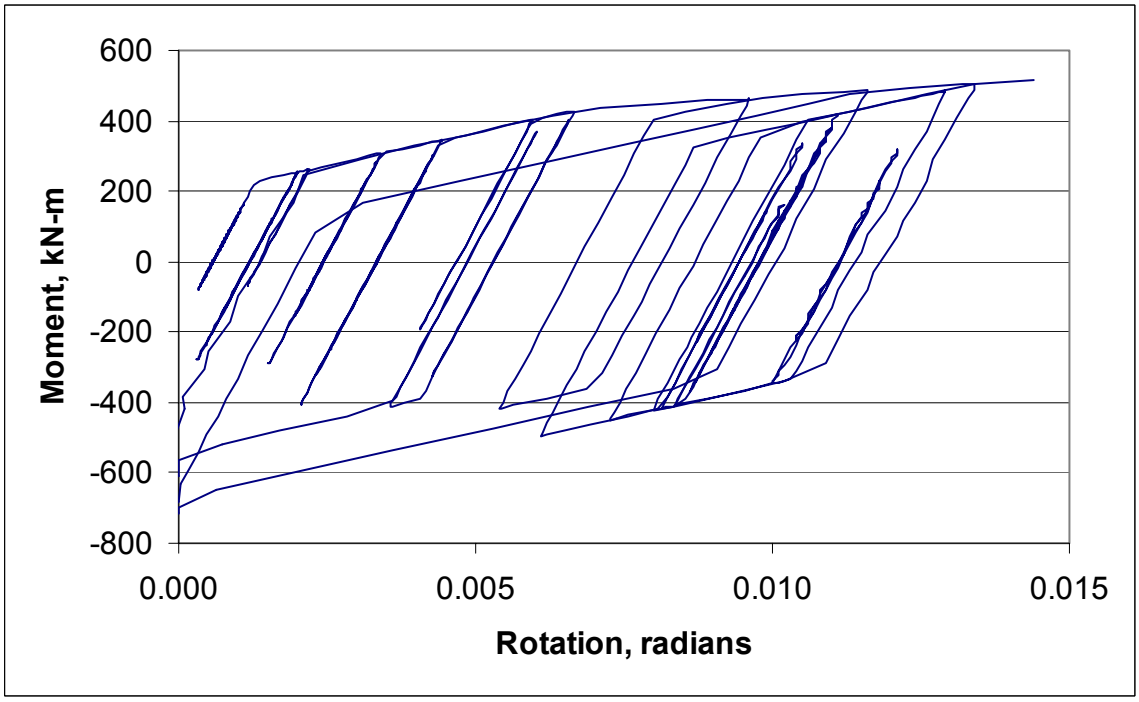

Figure B.29 Predicted BINP Task 2 cracked-section moment-rotation behavior using the quasi-static R = -0.3 J-R curve

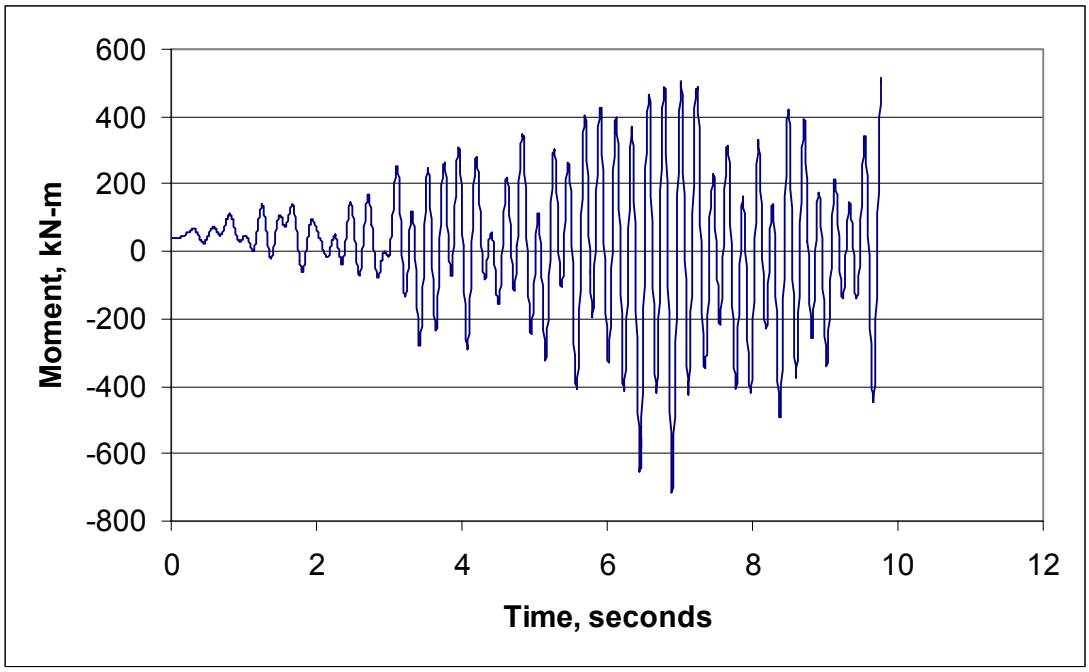

Figure B.30 Predicted BINP Task 2 moment-time behavior using the quasi-static R = -0.3 J-R curve

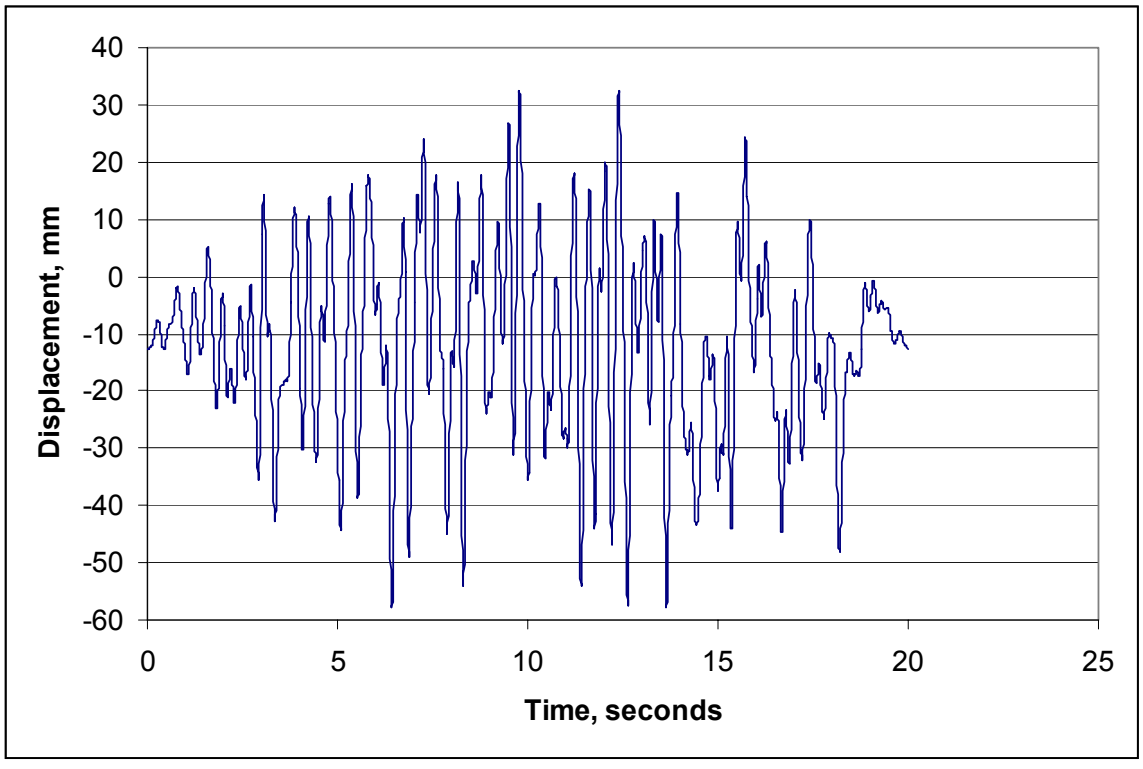

Figure B.31 The BINP simulated-seismic forcing function actuator displacement

B.1.4 Conclusions from Seismic Design Analysis

In terms of its character, the BINP seismic forcing function is similar to the IPIRG-2 seismic forcing function. Scaled to 3 SSE and respecting the fact that there is a -12.7 mm (0.5 inch) initial offset in the BINP forcing function, it is very difficult to tell the two functions apart, Figures B.31 and B.32. At the 3 SSE level, the IPIRG-2 seismic forcing function has a maximum displacement amplitude of 40.59 mm (1.6 inches) while the BINP forcing function has a maximum displacement amplitude of 45.03 mm (1.77 inches). Both forcing functions have the same "floor response" spectrum at the SSE level loading and 2-percent damping. Thus, at least superficially, they should have the same nominal potential for crack-driving force. Nonlinear analysis suggests otherwise.

As documented in this appendix, the BINP seismic forcing function was expected to have a significantly different effect on the cracked pipe than the IPIRG-2 seismic forcing function. By design, it had a much more negative stress ratio and thus, it should have induced more cyclic damage. Fortuitously, the BINP Task 2 test specimen used pipe DP2-A8ii, a heat of TP304 that has significantly more susceptibility to dynamic and cyclic effects than other heats tested in the IPIRG-2 program. The BINP Task 2 seismic loading, as it has been designed, should bring out these effects so that if the laboratory property J-resistance data translates into cracked pipe system fracture resistance degradation, it should be evident.

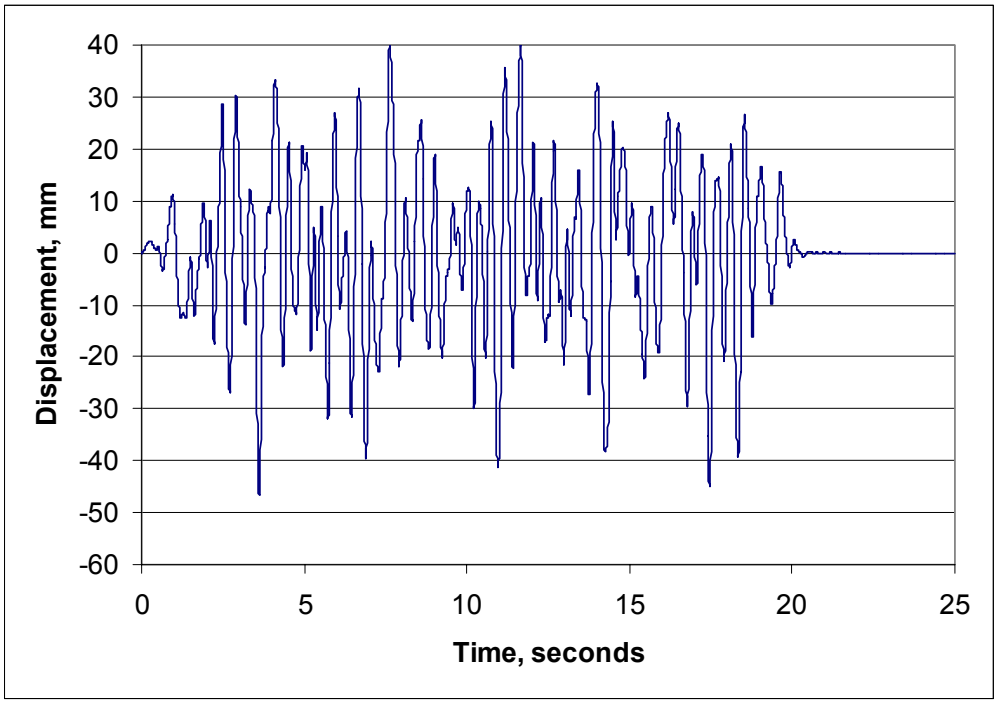

Figure B.32 The IPIRG-2 simulated-seismic forcing function actuator displacement at 3 SSE

B.2 RESULTS OF BINP SIMULATED SEISMIC PIPE-SYSTEM EXPERIMENT

The key results from the BINP simulated seismic pipe-system experiment are presented next. Table B.1 presents the test conditions, e.g., test pressure and temperature and test specimen and crack dimensions, for this experiment. Also included in Table B.1 is the maximum moment for the experiment.

Figure B.33 shows the actual actuator-time history from the experiment. Comparing the actual displacement-time history with the design displacement history in Figure B.31, one can see that the two forcing functions are very similar except the actual displacement-time history from the experiment does not reflect the initial static offset of –12.7 mm (0.5 inch) that was applied. The static offset was applied in the experiment, but the time = zero displacement value from the experimental record has been set to zero.

Figures B.34 and B.35 show the moment-time and moment-CMOD (crack-mouth-opening displacement) response for the experiment. Of particular note from Figure B.35 is the fact that there were significantly more plastic cycles in the early portion of the loading for this experiment than there were for the IPIRG-2 1-1 experiment, compare Figure B.35 with Figure B.2. Thus, it appears that the new BINP simulated seismic forcing function developed as part of this effort satisfied the basic objective of this task in that the forcing function resulted in a more cyclic damaging load history. The stress ratio, based on moment from Figure B.35, is -1.2 while the stress ratio, based on stress and accounting for the membrane stress due to the internal pressure, is –0.73. Consequently, the new BINP Task 2 seismic forcing function also satisfied the objective of creating the proper conditions for a forcing function with a significantly negative stress ratio.

Table B.1 Test conditions for BINP Task 2 simulated seismic pipe-system experiment

Mat'l	Outside Diameter, mm (inch)	Wall Thickness, mm (inch)	Crack Depth, mm (inch)	a/t	2c/BD	Test Temp., C (F)	Pipe Pressure, MPa (psi)	Max. Moment, kN-m (in-kips)
TP304	415.3 (16.35)	25.8 (1.016)	13.11 (0.516)	0.508	0.534	288 (550)	15.5 (2,250)	590 (5,220)

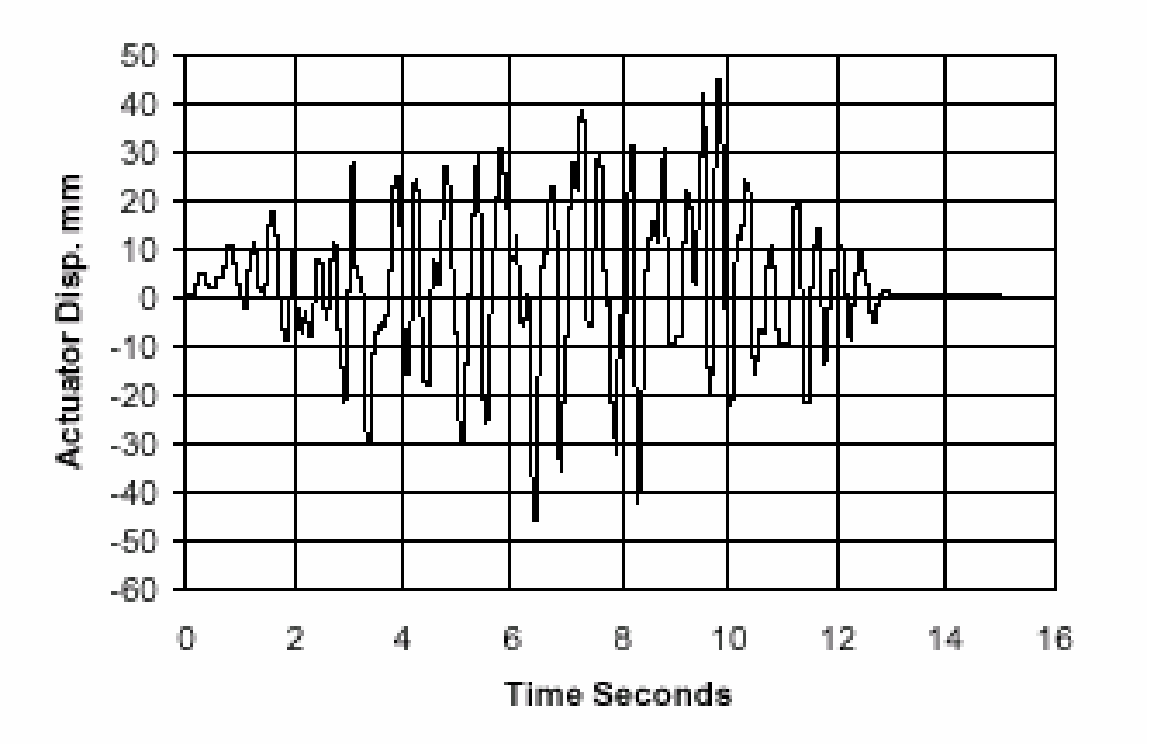

Figure B.33 Actuator displacement-time history for BINP Task 2 experiment

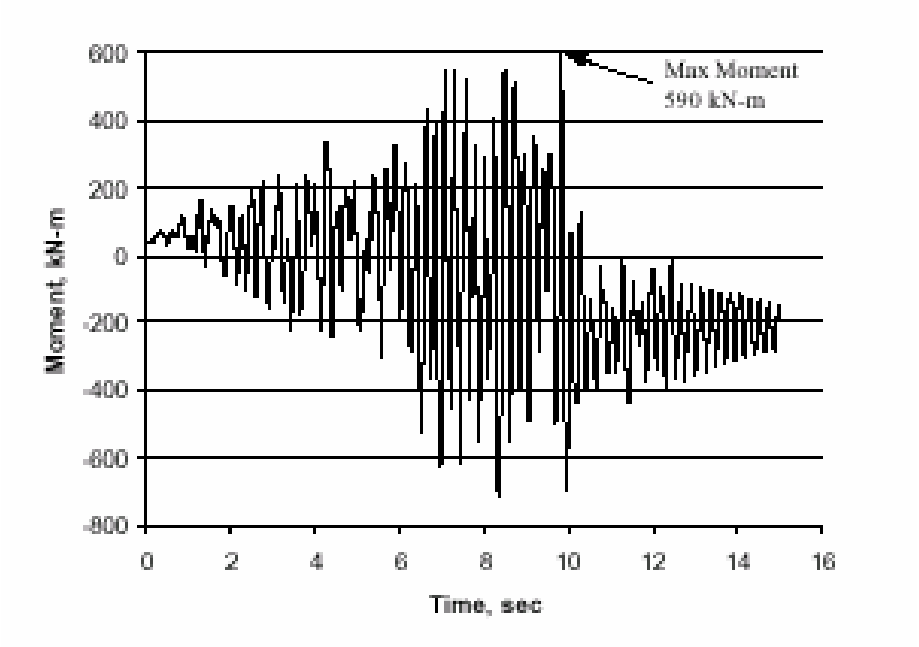

Figure B.34 Crack section moment-time response for BINP Task 2 experiment

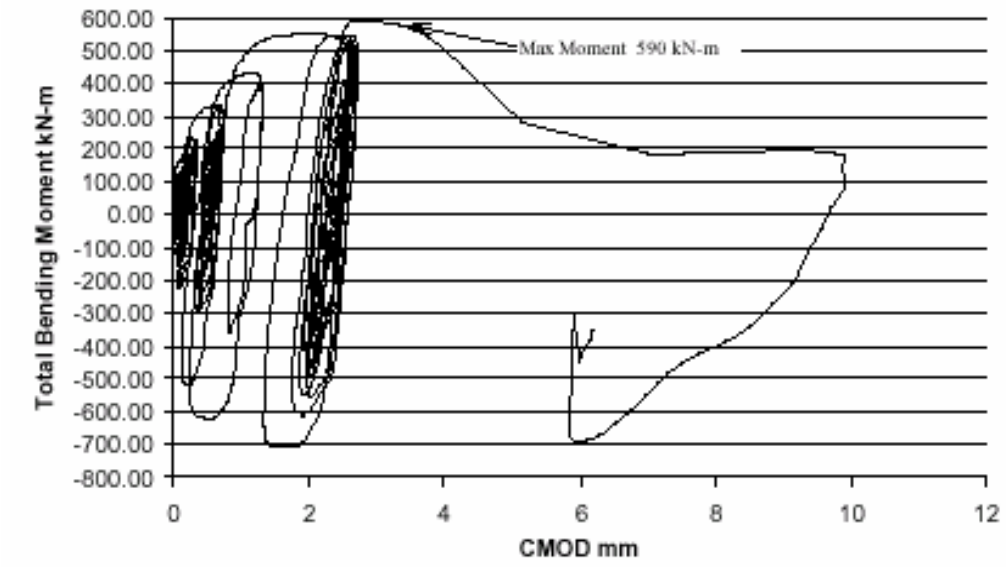

Figure B.35 Crack section moment-CMOD response for BINP Task 2 experiment

B.3 ANALYSIS OF RESULTS FROM BINP PIPE-SYSTEM EXPERIMENT WITH AN ALTERNATIVE SEISMIC LOAD HISTORY

To ascertain the impact of this alternative seismic forcing function on the fracture behavior of surface-cracked pipe-system experiments, comparisons with the other companion TP304 stainless steel surface-cracked pipe-system experiments conducted as part of the two IPIRG programs had to be made. The two companion stainless steel base metal pipe-system experiments were Experiment 1.3-3 from the

IPIRG-1 program and Experiment 1-1 from the IPIRG-2 program. The forcing function for Experiment 1.3-3 was a single frequency excitation superimposed over top an increasing displacement ramp, see Figure B.36. The forcing function for Experiment 1-1 was the IPIRG simulated seismic forcing function as shown in Figure B.1.

Table B.2 summaries the test conditions for the BINP Task 2 experiment as well as the two companion stainless steel pipe-system experiments. The test specimens for Experiments 1.3-3 from IPIRG-1 and the BINP Task 2 experiment were fabricated from the higher sulfur content heat of A8 (A8ii) while the test specimen for Experiment 1-1 from IPIRG-2 was fabricated from the lower sulfur content heat of A8 (A8i). The test conditions for each of the experiments were comparable (same test temperature [288 C (550F)], same test pressure [15.5 MPa (2,250 psi)], and nominally the same flaw size [50 percent of the pipe circumference in length and 66 percent of the pipe wall thickness in depth]). The major discriminator between the three experiments being the forcing function.

Table B.2 Test conditions for three stainless steel pipe-system experiments

Expt. Number	Mat'l Heat	OD, mm (inch)	Wall thickness, mm (inch)	Pressure, MPa (psi)	Test Temp., C (F)	a/t	2c/BD	Max. Moment, kN-m (in-kips)
BINP2	**A8ii (high S)**	**415.3 (16.35)**	**25.8 (1.016)**	**15.5 (2,250)**	**288 (550)**	**0.508**	**0.534**	**590 (5,220)**
1.3-3	**A8ii (high S)**	**415.8 (16.37)**	**26.2 (1.031)**	**15.5 (2,250)**	**288 (550)**	**0.647**	**0.552**	**426 (3,770)**
1-1	**A8i (low S)**	**417.1 (16.42)**	**25.5 (1.005)**	**15.5 (2,250)**	**288 (550)**	**0.632**	**0.527**	**598 (5,290)**

Table B.3 summaries the results from these experiments by presenting the maximum moment-carrying capacities in terms of the fracture ratios, i.e., the maximum stress from the experiments normalized by the Net-Section-Collapse (NSC) stress, accounting for the pressure induced membrane stress, see Equation B.1. This normalization process accounts for the slight differences in the pipe and crack sizes.

$$FR = \frac{\left(\sigma_m + \sigma_{b\_expt}\right)}{\left(\sigma_m + \sigma_{b\_NSC}\right)} \qquad \text{(B.1)}$$

where,

FR = Fracture Ratio
σ_m = membrane stress due to pressure
σ_{b_expt} = experimental bending stress
σ_{b_NSC} = Net-Section-Collapse predicted bending stress

Table B.3 Test results from three stainless steel pipe-system experiments in terms of fracture ratios

Expt. Number	Fracture Ratio
BINP2	**0.906**
1.3-3	**0.936**
1-1	**1.158**

In can be seen from Table B.3 that the moment-carrying capacity of the IPIRG-1 simulated seismic experiment (Experiment 1-1) is about 25 percent higher than the moment-carrying capacity of the other two stainless steel surface-cracked pipe-system experiments. One may want to immediately believe that this entire 25 percent reduction in moment-carrying capacity for the BINP Task 2 and the IPIRG-1 single-frequency experiments is due to cyclic effects

since the cyclic component of the moment-CMOD or rotation response is much more evident in Figure B.35 for BINP2 and Figure B.37 for Experiment 1.3-3 than it is for IPIRG-2 Experiment 1-1, see Figure B.2. However, the difference due to cyclic behavior is only half the story. As alluded to earlier, the test specimen for Experiment 1-1 was fabricated from the lower sulfur content, higher toughness heat of A8 (A8i) while the test specimens for the other two experiments were fabricated from higher sulfur content, lower toughness heat of A8 (A8ii), see Figure B.38. Sensitivity studies conducted as part of Reference B.5 showed that this difference in toughness may account for about a 15 percent difference in moment-carrying capacity. Consequently, the higher moment-carrying capacity of IPIRG-1 Experiment 1-1 is probably an artifact of both phenomena.

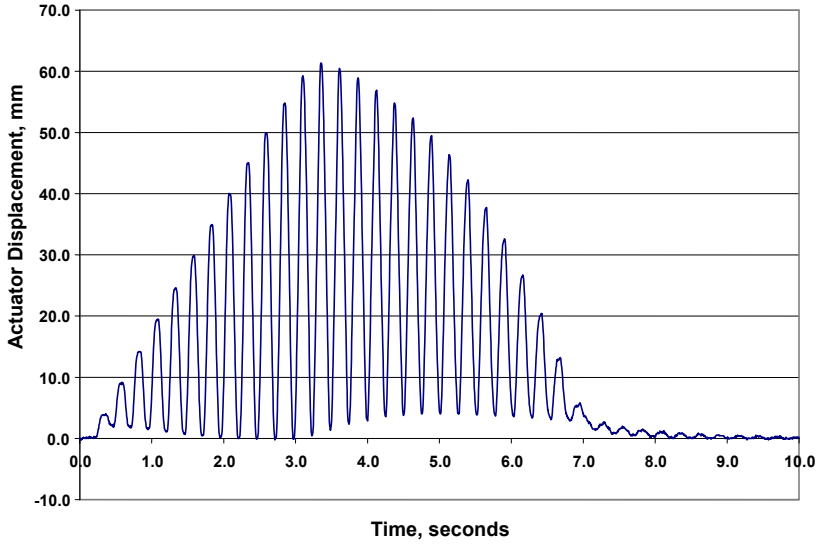

Figure B.36 Actuator displacement-time history for IPIRG-1 Experiment 1.3-3

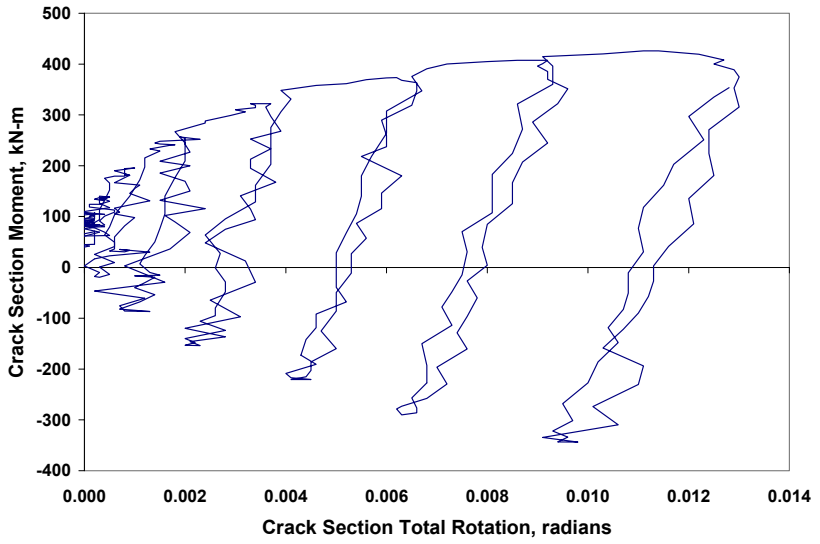

Figure B.37 Crack section moment-rotation response for IPIRG-1 Experiment 1.3-3

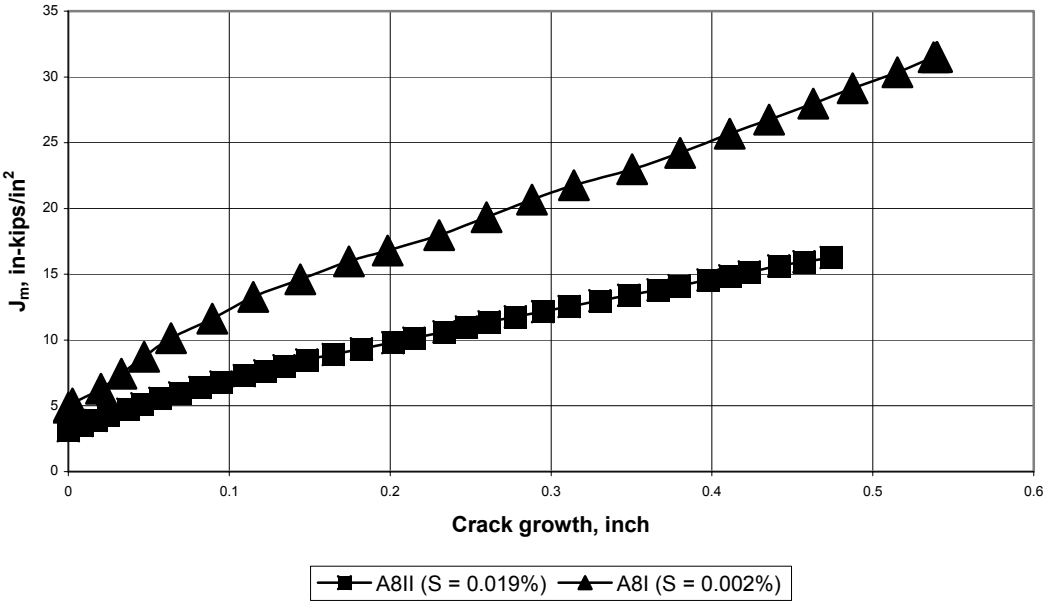

Figure B.38 Comparison of J-R curves for two heats of DP2-A8 stainless steel

Consequently the effect of cyclic loading on the moment-carrying capacity of these stainless steel base metal pipe-system experiments may result in only a 10 to 15 percent reduction. This does not seem to be that important of an effect, especially in light of the large factors of safety applied by such standards as ASME Section XI. However, the experiments conducted and analyzed so far have been for the case where the surface cracks were in rather high toughness stainless steel pipe materials for which limit load conditions probably prevailed and the effects of toughness degradation due to cyclic loading may not be that significant. Consequently, the question that needs to be answered is what would be the effect if these experiments and analyses had been conducted using a lower toughness ferritic material or a lower toughness stainless steel flux weld, maybe in a larger diameter pipe for which limit load is less likely to occur.

In order to address this question, additional J-estimation scheme analyses were conducted. For these additional analyses, the SC.TNP1 method was used since past studies have shown that this method is the most accurate predictor of the moment-carrying capacity of surface-cracked pipe.

Two sets of analyses were conducted. For the first set, J-estimation scheme analyses were conducted for a 16-inch diameter, Schedule 100 stainless steel pipe, with a crack in the base metal 25 percent of the pipe circumference long and 50 percent of the pipe wall thickness deep. Two analyses were conducted. For one, the quasi-static, monotonic J-R curve for Heat A8i was used. For the other, a J-R curve that had been uniformly reduced for all values of Δa by a factor of 2.5 was used. This factor of 2.5 was chosen in that the J-R curve for A8i for the monotonic, R = -1 loading condition was only 40 percent of the J-R curve for the quasi-static, monotonic loading condition, see Figure B.39. For this stainless steel material, with its relatively high toughness level, limit-load conditions most likely exist for this diameter pipe.

For the second set of J-estimation scheme analyses a case was chosen for which limit-load conditions most likely did not exist. For these analyses, 32-inch diameter main steam line was

chosen for analysis. In this case, the crack was in a lower toughness ferritic weld. Both quasi-static, monotonic J-R curve data and quasi-static, cyclic (R = -1) J-R curve data were used in the SC.TNP1 analyses. The quasi-static data were obtained from weld material DP2-F29W, a ferritic pipe weld used in a number of past pipe experiments. The cyclic J-R curve data were obtained by multiplying each of the J values in the quasi-static, monotonic J-R curve file by 0.4. In this manner, it will be possible to ascertain if the reduction in moment-carrying capacity is different for the case where limit-load conditions exist and for the case where elastic-plastic fracture governs.

Figure B.40 is a plot of the resultant moment-rotation curves from the SC.TNP1 analyses for the stainless steel case where limit-load conditions most likely exists. As can be seen, the maximum moment for the cyclic case was about 81 percent of the maximum moment for the monotonic case. Figure B.41 is a plot of the resultant moment-rotation curves from the SC.TNP1 analyses for the larger diameter, ferritic weld case where EPFM most likely governs. For this case, the maximum moment when using the cyclic J-R curve was only about 66 percent of the maximum moment when using the monotonic J-R curve. Thus, it appears cyclic loading may be a more important factor to consider for cases where EPFM governs.

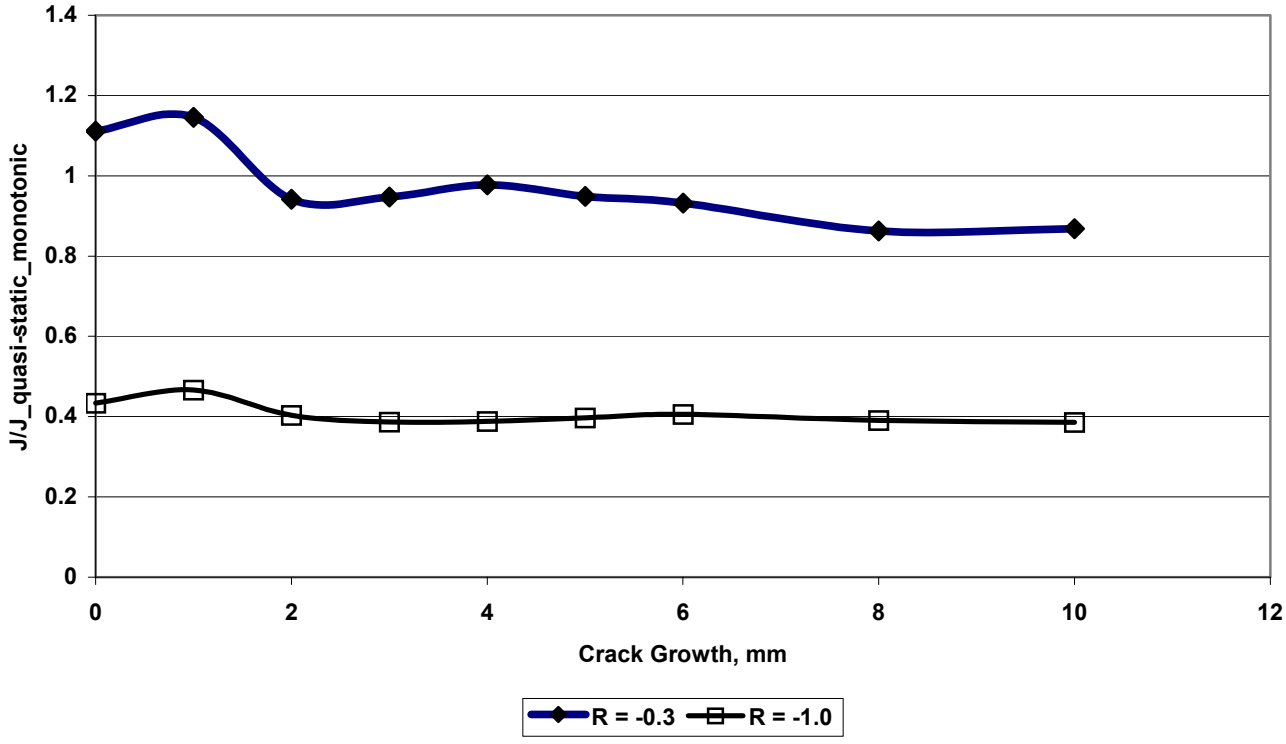

Figure B.39 Ratio of quasi-static cyclic J values to J for quasi-static monotonic loading as a function of crack growth ( ) a)

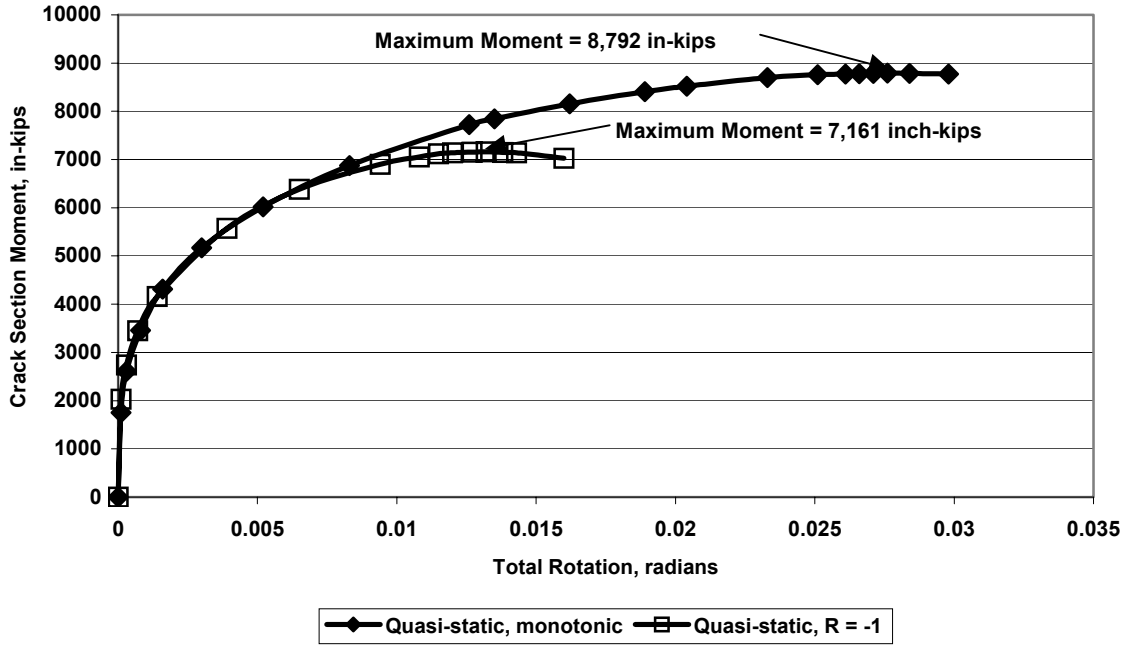

Figure B.40 Predicted moment-rotation behavior for 16-inch diameter schedule 100 stainless steel pipe for quasi-static monotonic and quasi-static cyclic (R = -1) J-R curves

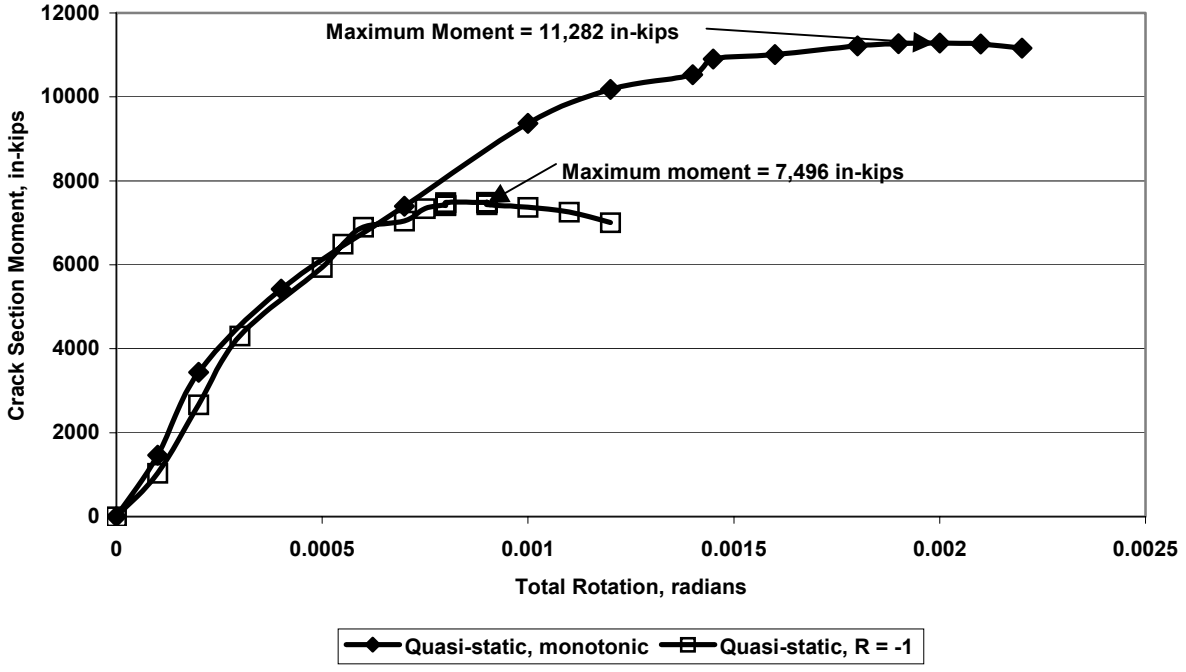

Figure B.41 Predicted moment-rotation behavior for 32-inch diameter carbon steel pipe for quasi-static monotonic and quasi-static cyclic (R = -1) J-R curves

B.4 REFERENCES

B.1 Olson, R., Scott, P., and Wilkowski, G., "Design of the IPIRG-2 Simulated Seismic Forcing Function," NUREG/CR-6439, February 1996.

B.2 Rahman, S., Olson, R., Rosenfield, A., and Wilkowski, G., "Summary of Results From the IPIRG-2 Round-Robin Analyses," NUREG/CR-6337, January 1996.

B.3 Rudland, D., Brust, F., and Wilkowski, G., "Fracture Toughness Evaluations of TP304 Stainless Steel Pipes," NUREG/CR-6446, February 1997.

B.4 Olson, R., Wolterman, R., Wilkowski, G., and Kot, C., "Validation of Analysis Methods for Assessing Flawed Piping Subjected to Dynamic Loading," NUREG/CR-6234, August 1994.

B.5 Scott, P., Olson, R., and Wilkowski, G., “Development of Technical Basis for Leak-Before-Break Evaluation Procedures,” NUREG/CR-6765 May 2002.